


# Stimuli-responsive active materials for dynamic control of light field

Ren Zheng<sup>1</sup> | Yang Wei<sup>1</sup> | Zi-Chen Zhang<sup>1</sup> | Ze-Yu Wang<sup>1</sup> | Ling-Ling Ma<sup>1</sup>  |  
Yu Wang<sup>1</sup> | Ling Huang<sup>2</sup> | Yan-Qing Lu<sup>1</sup>

<sup>1</sup>National Laboratory of Solid State Microstructures, Key Laboratory of Intelligent Optical Sensing and Manipulation, College of Engineering and Applied Sciences, Collaborative Innovation Center of Advanced Microstructures, Nanjing University, Nanjing, China

<sup>2</sup>State Key Laboratory of Chemistry and Utilization of Carbon Based Energy Resources College of Chemistry, Xinjiang University, Urumqi, China

## Correspondence

Ling-Ling Ma, Yu Wang, Ling Huang and Yan-Qing Lu.

Email: [malingling@nju.edu.cn](mailto:malingling@nju.edu.cn), [yuwang87@nju.edu.cn](mailto:yuwang87@nju.edu.cn), [iamlhuang@njtech.edu.cn](mailto:iamlhuang@njtech.edu.cn) and [yqlu@nju.edu.cn](mailto:yqlu@nju.edu.cn)

## Abstract

The increasing demand for the multidimensional and dynamic control of light has spurred the development of stimuli-responsive, reconfigurable, and programmable optical systems. Liquid crystals (LCs), which combine liquid-like stimuli-responsiveness and crystal-like orientational ordering, have emerged as highly appealing soft materials. Owing to their exceptional optical performance and programmable functionalities, they are becoming incredibly important materials in active planar optics and photonics. Additionally, silk proteins, luminescent materials, and metasurfaces exhibit dynamic optical properties, enabling remarkable multifunctional applications. This review focuses on the advancements in stimuli-responsive materials, including LCs, silk proteins, luminescent materials, and active metasurfaces as well as some of these materials paired with LCs. Their attractive tunable applications in optics and photonics, along with the great potential for the future development of active optical systems, are also emphasized.

## Keywords

light modulation, optical applications, stimuli-responsive materials, tunability

## 1 | INTRODUCTION

Light control is essential for advancing scientific knowledge, enabling technological breakthroughs, and improving quality of life. Its applications span the spectrum from basic scientific research to everyday technologies, impacting fields such as communications,<sup>[1]</sup> energy,<sup>[2]</sup> displays,<sup>[3]</sup> imaging,<sup>[4]</sup> and sensing.<sup>[5]</sup> In order to attain versatile and efficient manipulation of optical characteristics, such as wavelength/frequency, amplitude, polarization, phase, and angular moment, the incorporation of artificial microstructure design is imperative for optoelectronic devices. In recent decades, the increasing demand for advanced optical applications has led to heightened expectations for active and adaptive optics, and therefore, extensive endeavors have been dedicated to the exploration of dynamically tunable optical materials.<sup>[6]</sup>

Stimuli-responsive active materials have drawn great attention in this context because they exhibit excellent characteristics, such as elasticity,<sup>[7]</sup> flexibility,<sup>[8]</sup> conformability,<sup>[9]</sup> self-healing,<sup>[10]</sup> energy absorption,<sup>[11]</sup> tunability,<sup>[12]</sup> and so on. Liquid crystals (LCs) representing one of the most attractive soft materials are a phase of matter that exhibits properties of both liquids and crystals.<sup>[13]</sup> LC molecules have a characteristic rod-like or disc-like shape and typically consist of organic compounds. They align themselves in a specific manner known as “director” under the influence of external stimuli, such as heat, light, electric field, magnetic field, mechanical stress, humidity, etc.<sup>[6e,14]</sup> The orientational order of LCs gives rise to unique anisotropic optical, electrical, and mechanical properties governed by the structural arrangement.<sup>[15]</sup> One of the most well-known applications is LC displays (LCDs) in televisions, computer monitors, and

This is an open access article under the terms of the [Creative Commons Attribution](https://creativecommons.org/licenses/by/4.0/) License, which permits use, distribution and reproduction in any medium, provided the original work is properly cited.

© 2023 The Authors. *Responsive Materials* published by John Wiley & Sons Australia, Ltd on behalf of Southeast University.

mobile devices. Beyond displays, LCs find applications in diverse fields, such as optical communications, light engineering, sensors, and drug delivery systems.<sup>[16]</sup> Their unique properties make them ideal for designing optical devices that can respond to external stimuli, exhibit tunable behavior, and modulate light.<sup>[6d,17]</sup> Ongoing research in the field of LCs continues to unlock the potential for advancements in both material science and information technology.

Silk proteins are a class of structural proteins found in silk fibers produced by certain insects, such as *Bombyx mori* silkworms.<sup>[18]</sup> They are known for their exceptional material characteristics, including mechanical flexibility,<sup>[19]</sup> biocompatibility,<sup>[20]</sup> biodegradability,<sup>[21]</sup> stimuli-responsiveness,<sup>[22]</sup> favorable optical properties,<sup>[23]</sup> and ease of functionalization.<sup>[24]</sup> Furthermore, by employing techniques, such as bottom-up self-assembly and top-down nanostructuring, silk proteins can organize themselves into periodic arrays or patterns that possess the ability to manipulate light at multiple scales.<sup>[12a,22b,25]</sup> This capability enables the creation of photonic crystals, diffractive gratings, and other optical elements with exceptional and distinctive properties. More interestingly, silk proteins are splendid candidates for active optics owing to their dynamic responsiveness to a diverse range of environmental stimuli.

Another important optical material with stimuli-responsiveness is luminescent materials, also called phosphors. Luminescent materials are a substance that converts certain types of excitation energy into electromagnetic (EM) radiation, for example, light. The emitted light covers not only the visible region but also other regions, including ultraviolet (UV) and near-infrared (NIR) light.<sup>[26]</sup> This wide range of optical responses makes luminescent materials play a vital role in many aspects, including lighting, display, catalysis, energy, life sciences, etc.<sup>[27]</sup> Therefore, precise control over the optical function of luminescent materials is of fundamental importance for their applications and has always been the focus of research.<sup>[28]</sup> Fortunately, luminescent materials have been found to be responsive to various external stimuli and can be utilized for effective manipulation of optical properties.<sup>[29]</sup>

Metamaterials are synthetic materials with unique properties that cannot be found in naturally occurring materials.<sup>[30]</sup> They are typically composed of subwavelength structures called meta-atoms, which are carefully designed to manipulate light and other EM waves in ways that are impossible with conventional materials.<sup>[6a]</sup> Recently, dynamically tunable metasurfaces have also been developed.<sup>[31]</sup> These metasurfaces can actively change their optical properties in real time, offering even greater control over light manipulation. By integrating external stimuli, such as temperature variations, these metasurfaces can dynamically modify their responses to incident light.<sup>[32]</sup>

To date, substantial advancements have been achieved in the development of dynamically tunable optical platforms based on these stimuli-responsive active materials, and there have been some excellent reviews summarizing these advancements.<sup>[33]</sup> However, there remains a notable gap in the

literature, as a comprehensive review encompassing these mainstream stimuli-responsive materials has not yet been compiled. Additionally, in recent years, there has been a proliferation of research regarding the integration of LCs with other active materials to achieve distinctive or multiple tunable optical functionalities; nevertheless, such efforts have yet to be systematically summarized.

Here, we focus on the recent advancements in actively tunable optical materials (Figure 1), specifically LCs (Section 2), silk proteins (Section 3), luminescent materials (Section 4), and metasurfaces (Section 5). We discuss various aspects of these materials, ranging from their material properties and structural control to stimuli-responsive behavior as well as optical functionalities. We emphasize the remarkable significance of these stimuli-responsive materials, which hold notable promise for future advancements in optics in various scientific, technological, and industrial domains, especially in optical communication, optical computing, optical imaging, photovoltaics, holography, optical spectroscopy, nonlinear photonics, quantum optics, etc.

## 2 | DYNAMICALLY RECONFIGURABLE LC

LCs are a promising class of optical materials with unique stimuli-responsive properties.<sup>[6c,34]</sup> They exist in a distinct phase between the crystalline solid state and the isotropic liquid state, known as the LC phase.<sup>[14a]</sup> This thermodynamically stable state combines the fluidity of liquids with the optical/dielectric anisotropy of crystals.<sup>[6d,15b]</sup> In general, LCs can be classified into different mesophases, including the nematic, cholesteric, blue phase, and lamellar smectic phase. Nematic LCs (NLCs) exhibit long-range orientational ordering, which results in distinct anisotropic physical properties. These properties can be modified further by varying the composition of the LCs.<sup>[35]</sup> For cholesteric LCs (CLCs), molecules self-assemble into a helical arrangement, which is characterized by their pitch ( $p$ ) and handedness. The pitch refers to the distance over which the director field rotates by a complete turn of 360°. This chiral structure imparts a distinctive circular-polarization selectivity to broadband Bragg reflection when the incident light propagates along the helical axis.<sup>[16a,36]</sup> Additionally, the blue phase represents a remarkable state featuring cubic lattices composed of double twist cylinders. This phase usually occurs in systems with high chirality and within a limited temperature range.<sup>[37]</sup> The smectic phase is classified as a mesophase and distinguished by its organized lamellar structure. Smectic LCs (SLCs) exhibit both the long-range orientational and positional order with the long axes of the molecules being either perpendicular or tilted to the layer plane. Various topological superstructures have been observed in the SLCs under different external conditions.<sup>[38]</sup> Polymeric LCs, such as LC elastomers (LCEs) and LC networks (LCNs), exhibit macroscopic deformation when stimulated by an external thermal field. When heated above

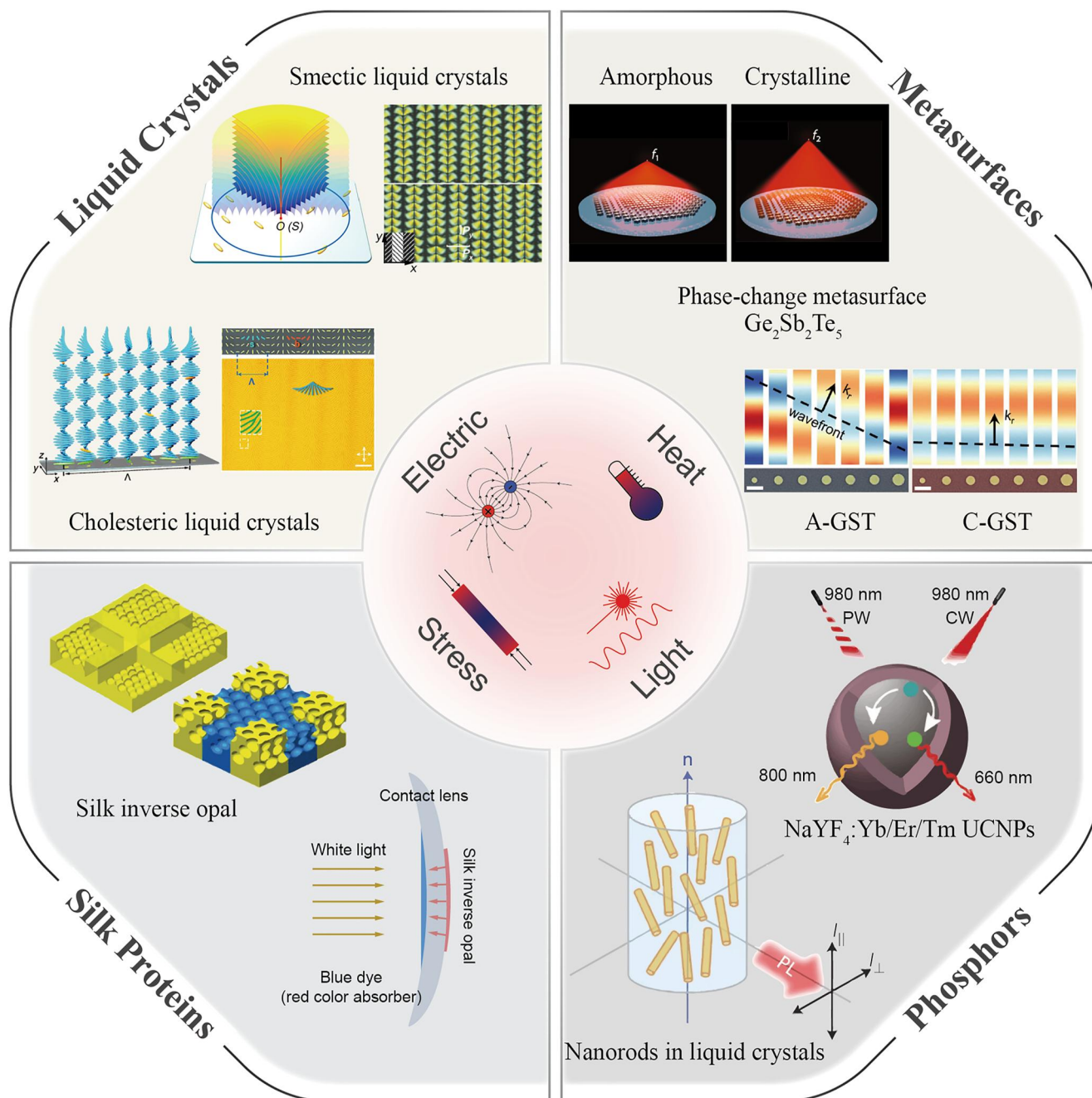


**FIGURE 1** Schematics of material structures and corresponding stimuli-responsive performances of liquid crystals, silk proteins, phosphors, and metasurfaces under various external stimuli. Reproduced with permission.<sup>[17g]</sup> Copyright 2017, John Wiley and Sons. Reproduced with permission.<sup>[14b]</sup> Copyright 2021, The American Association for the Advancement of Science. Reproduced with permission.<sup>[12a]</sup> Copyright 2019, John Wiley and Sons. Reproduced with permission.<sup>[22b]</sup> Copyright 2017, National Academy of Sciences. Reproduced with permission.<sup>[29a]</sup> 2017, Springer Nature. Reproduced with permission.<sup>[29b]</sup> 2022, Springer Nature. Reproduced with permission.<sup>[32c]</sup> Copyright 2022, Springer Nature. Reproduced with permission.<sup>[32e]</sup> Copyright 2021, Springer Nature.

the glass transition temperature, the in-built orientational order of LCs reduces, resulting in contraction along the LC director and elongation perpendicular to the director.<sup>[7,17c]</sup>

The ease of alignment along predefined directors and facile structure switching under external fields have endowed LCs with attractivity in many fields.<sup>[6d,6f,14b,16a,39]</sup> As an adaptive response to external stimuli (electric field,

magnetic field, heat, light, mechanical stress, etc.), LC-based adaptive planar optics has gained remarkable attention. With external stimuli, the dynamic manipulation of LC structures is important for active optical applications, further leading to more advanced optical functionalities. In the following paragraphs, we will discuss the recent progress in stimuli-responsive LCs and their active optical applications.

## 2.1 | Thermally sensitive LCs

Thermochromic LCs, a unique class of materials, exhibit alterations in their textures or optical properties in response to temperature variations. The behavior of thermochromic LCs is based on their phase-transition characteristics. These materials exhibit different molecular arrangements at different temperatures, leading to distinct LC phases, including the nematic phase, smectic phase, cholesteric phase, blue phase, etc. One of the key features of thermochromic LCs is their reversible nature. As the temperature increases or decreases, the LCs shift between different phases, resulting in a visible and reversible change in their optical performances. This property makes them suitable for a range of applications, such as temperature sensing, thermal mapping, temperature-dependent coatings, smart windows, and even visual indicators for temperature variations in various systems. Besides the temperature, temperature programming and functional dopants affect the LC structures.<sup>[17c,17g,38,39b,40]</sup>

Across the nematic–smectic (N–S) phase transition, toric focal conic domain (TFCD) arrays of SLC can be easily generated under antagonistic anchoring conditions. The thermodynamic process will determine the evolution of TFCDs.<sup>[38,41]</sup> Wu et al.<sup>[38]</sup> demonstrated two distinct topological defects in the N phase by varying the cooling rate. One was a pure point defect array, and the other was unidirectional disclination lines. After crossing the N–S phase transition, two ordered TFCD arrays with different distributions and lattice sizes could be obtained because of the inheritance of the orientational order. In addition, the simultaneous tailoring of the geometry (domain size, shape, and orientation) and clustering characteristics of FCDs have been achieved and the 3D smectic layer origami was accomplished via a 2D preprogrammed photoalignment film. The unique symmetry breaking of resultant superstructures combined with the optical anisotropy of the LCs induces an intriguing polarization-dependent diffraction.<sup>[17g]</sup> Furthermore, a new LC phase, ferroelectric nematic ( $N_F$ ), was discovered with temperature sensitivity.<sup>[40e]</sup> With phase transition from N to  $N_F$  upon cooling, the  $N_F$ LCs showed a uniaxial phase and spontaneous polarization along the director, different from NLCs.<sup>[40a,40d,42]</sup> The key evidence for this result was the first observation in an NLC of the defining characteristics of ferroelectricity: spontaneous polar domains of opposite signs of polarization separated by distinct domain boundaries, without applied electric field.<sup>[42a]</sup> In addition, thermoresponsive helical superstructures can be formed by doping the LC host with temperature-responsive chiral dopants. The tunable reflected colors of CLCs with thermo-sensitive chiral dopants were demonstrated, and the center wavelength was remarkably tuned from 780 to 380 nm with a mere 3°C temperature increase from room temperature.<sup>[40c]</sup> For multiple stimuli, such as light irradiation and heat, the halogen-bonded chiral switch can endow the CLC structure with tunability and the optical reflected color across the entire visible spectrum.<sup>[39d]</sup> Blue phase LCs

are also of high chirality and emerge in the narrow temperature range of a few degrees centigrade, which is an obstacle for practical applications. Furthermore, a temperature range of 280°C and blue phase range preservation more than 132°C after excluding the frozen glassy state were observed by introducing a series of tailored uniaxial rod-like mesogens into the blue phase system, exhibiting the crucial role of ultrastable 3D nanostructures and tunable photonic applications.<sup>[37a]</sup>

The corresponding optical applications can be implemented based on the aforementioned thermoresponsive structure of LC systems. Ma et al.<sup>[41]</sup> designed self-assembled asymmetric LC microlenses with multifocal functionality and polarization selectivity for the demonstration of four-dimensional visual imaging (Figure 2a). The capabilities of demultiplexing of depth/polarization information were also presented in a single snapshot, which may unlock a variety of revolutionary apparatuses and lighten extensive applications. For chiral LCs, both the linear and nonlinear optical effects can be fulfilled by tuning thermoresponsive LC structures. Zhang et al.<sup>[39b]</sup> applied two thermal-responsive CLC components with opposite chiralities to perform dynamic optical detection. The wavelength and spin angular momentum of incident light can be detected by spin-selective Bragg reflection of CLCs, and orbital angular momentum of  $\hbar$  is detected by introducing a distorted grating. For the ferroelectric LCs, during the temperature range of  $N_F$ LCs, a universal phase-matching theory was developed and the nonclassic chirality-sensitive phase-matching condition in the polarization helices was achieved.<sup>[43]</sup> Additionally, Zheng et al.<sup>[17c]</sup> proposed an active smart LC actuator with programmable bending motions and autonomous self-sustained waddling oscillations in response to heat. Combining these macroscopic actuation and optical microstructures (including q-plate, Fresnel lens, etc.) achieved dynamic 2D beam steering and self-sustained light field modulation, which provided new insight into smart actuators with distinctive functions of thermo-mechanical-optical transduction (Figure 2b).

## 2.2 | Light-driven LCs

Compared to heat stimulus, light stimulus on LC structures possesses distinct advantages with high spatial and temporal precision even for remote and digital control.<sup>[15c,44]</sup> Various features (such as wavelength, intensity, polarization, etc.) of light would have different effects on tuning the LC structure and optical performance.<sup>[6f,14b,36,44c,45]</sup>

LCs are endowed with structural tunability by light when doped with photoresponsive matter with photochemical or photothermal effects. The azo-chiral dopants, azo-dyes, and other photoresponsive materials can undergo photoisomerization upon a given wavelength of light. Once the azo-chiral dopants are doped in the LC hosts, a helical superstructure can be formed.<sup>[15d,34f,46]</sup> In addition, this helical superstructure can be tuned with the chiral dopant



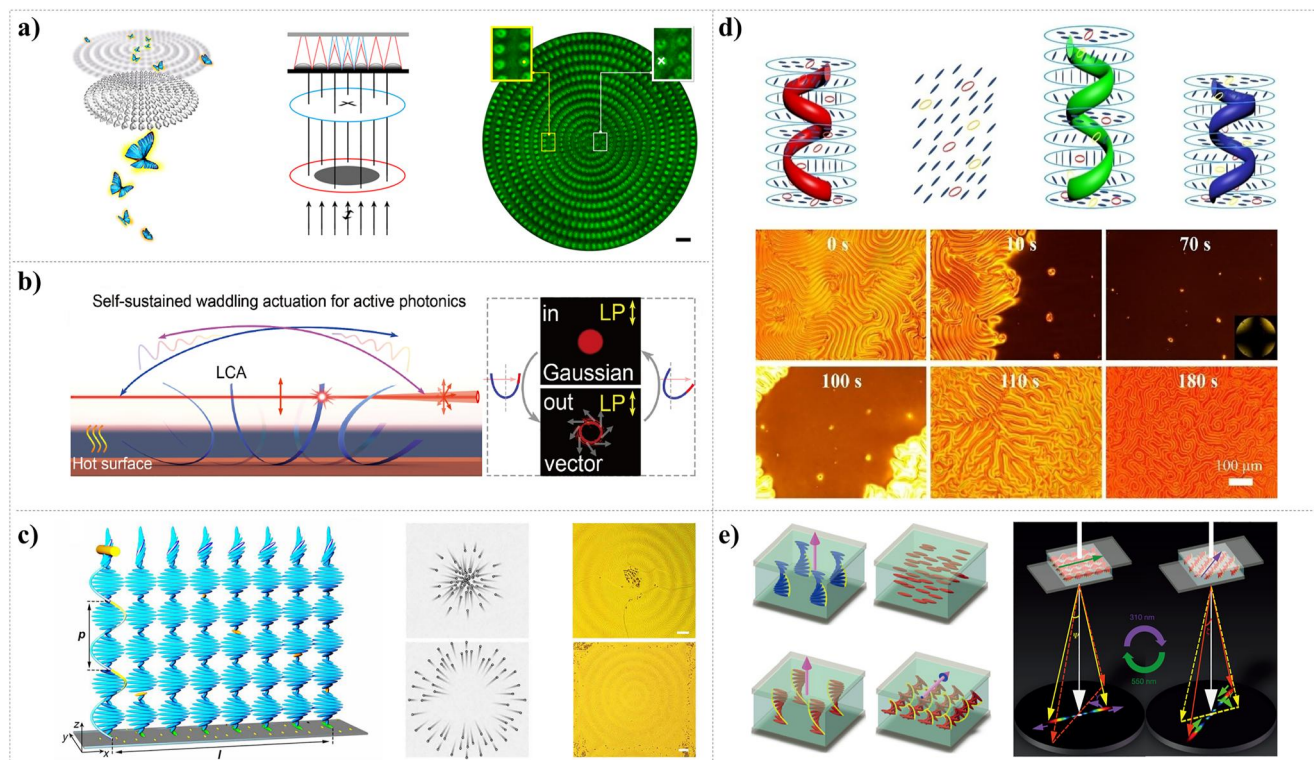


**FIGURE 2** Performances of thermal and light stimuli-responsive LCs. (a) Depth/polarization information demultiplexing of microlens. Scale bar: 20  $\mu\text{m}$ . Reproduced with permission.<sup>[41]</sup> Copyright 2019, American Chemical Society. (b) Dynamic Gaussian/vector beams switch by self-sustained waddling actuation. Reproduced with permission.<sup>[17c]</sup> Copyright 2023, John Wiley and Sons. (c) Semi-free CLC film with helical configuration for converging and diverging the particles. Scale bar: 50  $\mu\text{m}$ . Reproduced with permission.<sup>[14b]</sup> Copyright 2021, The American Association for the Advancement of Science. (d) Visible-light-driven handedness inversion of CLC mixture. Scale bar: 100  $\mu\text{m}$ . Reproduced with permission.<sup>[47]</sup> Copyright 2023, John Wiley and Sons. (e) Chiral switch of the helical superstructure and two-dimensional beam steering. Reproduced with permission.<sup>[44d]</sup> Copyright 2016, Springer Nature. CLC, cholesteric LC; LCs, liquid crystals.

undergoing *trans-cis* isomerization under UV irradiation and reversing to the initial *trans*-isomerization with visible light irradiation or heat. Ma et al.<sup>[14b]</sup> mimicked the motion of bacteria flagella using the light-driven evolution of a self-organized periodic arch pattern. They realized programmable self-propelling actuators via specific molecular assembly within a photoresponsive cholesteric medium (Figure 2c). Through rationally presetting alignments, parallel transport of microspheres in customized trajectories was demonstrated, including convergence, divergence, gathering, and orbital revolution. Moreover, the handedness inversion of CLCs upon photoisomerization by light is interesting. Upon exposure to visible light of different wavelengths, CLCs, doped with chiral molecular switches with terminal bromo atoms, were demonstrated to undergo reversible handedness inversion by Wang et al.<sup>[46]</sup> Furthermore, they first demonstrated that linking the binaphthyl to *ortho*-positions of azobenzene and shorter substituents to the 6,6'-positions of binaphthyl realized handedness inversion in CLCs.<sup>[47]</sup> Upon irradiation with 530 nm light, *trans*-to-*cis* photoisomerization and photostationary state were achieved, and reverse isomerization was realized by 440 nm light, where the light-driven handedness inversion of CLCs was performed (Figure 2d). Upon light of multiple wavelengths,

such as sunlight, a chronotropic device has also been achieved, showing a feasible sunlight-driven approach. Besides the wavelength, the intensity of light will influence the LC structure. Kuentler et al.<sup>[48]</sup> fabricated LCE waveguides with doping AuNPs in localized regions, where reversible photothermal deformation by plasmonic absorption of waveguided light occurred. As the light intensity increased, the bending angle raised smoothly owing to the heat generation, which reached 13° upon 30 s exposure to (532 nm) light at a certain power. In addition to the wavelength and intensity of light, the polarization of light functions as the controlling parameter to the LC structure greatly, when dichroic dyes are used for the photothermal effect. Polarization serving as an additional manipulation degree of freedom for LC actuation manipulation was demonstrated by dichroic dye RL002.<sup>[44c]</sup> The photothermal effect differed with the angle between the polarization direction of the linearly polarized incident light and the orientation of dichroic dye, where maximum and minimum were at 0° and 90°, respectively.

Additionally, the dynamic structures of LCs have promoted the development of active optics and photonics remarkably. By continuously tuning the pitch and handedness of CLCs, Chen et al.<sup>[16a]</sup> achieved ultra-broadband

(over 1000 nm) tunable planar optical elements with light stimulation, where a photoresponsive azobenzene chiral molecular and an opposite chiral dopant were applied. For virtual reality (VR) and augmented reality, photosensitive azobenzene and dichroic dye can be applied for much faster response time. With electric field assistance, the LC structure reversal time can be reduced to a few milliseconds.<sup>[45b]</sup> For orientation disorder, phase defects, fatigue resistance, and thermal instability of photosensitive CLCs, improving the stability of the helical structure and optical performance has great demand. Owing to the bistable limitation of azobenzene-based chiral switches, the tunable spectrum from the NIR region to the visible spectrum simultaneously is challenging. To address this problem, Qin et al.<sup>[49]</sup> designed CLCs consisting of photoresponsive tristable chiral switch to achieve excellent performance in RGB and black reflective displays, where selective reflection was tuned from the visible to the NIR spectrum region around 1430 nm. Besides, by synthesizing the axially chiral molecular switch (*S*, *S*)-**D4**, Li's group achieved the 3D manipulation of the CLCs' helical axis and handedness inversion, where the helical axis experienced the reversible transition from perpendicular to parallel, and in-plane rotation in sequence (Figure 2e).<sup>[44d]</sup> This caused the wide-area and reversible 2D beam steering activated by light. In addition, Zheng et al.<sup>[36]</sup> developed dissymmetric chiral photosensitive diarylethene switches, which were stable and lasted for 4 h after UV irradiation, by a sterically hindered ethene bridge and the unique feature of light-induced reversible transformation. For dynamic helical transformation, it is a great candidate for reversible and programmable light applications, and anti-counterfeiting, displays, and labeling technologies have been achieved. Interestingly, the helical structure of LCE fibers also functions in photomechanical transduction. Hu et al.<sup>[44a]</sup> created a phototunable helix formation self-oscillating system with the photothermal effect of graphene. Under the NIR light exposure, laser modulation can be achieved by hanging a mirror reflector on an LCE helical fiber. The photomechanical actuation allows one-dimensional scanning with horizontal and vertical angular tuning. In summary, phototunable LCs enable photo-mechanical-optical transduction.

### 2.3 | Electrically switchable LCs

LC molecules are of dielectric anisotropy, and under the electric field, they would be reoriented. Richard Williams first discovered an interesting electro-optic characteristic that under the external electric field, a regular pattern was found due to the reorientation of NLCs in 1962.<sup>[50]</sup> Furthermore, LCs with feasibility for display devices were demonstrated, which were a forerunner of the LCD. Later, both the intensity and frequency of the applied electric field showing great influence of LC realignment were discovered, thereby indicating a possible pathway to binary responsiveness.<sup>[17d,17e,34g,51]</sup>

According to their dielectric constants, NLCs can be separated into two types. One type is with positive dielectric anisotropy, and its dielectric constant along the director ( $\epsilon_{//}$ ) is greater than that perpendicular to the director ( $\epsilon_{\perp}$ ). With an applied electrical field higher than the critical value, the LC molecules realign their directors parallel to the direction of the electrical field ( $\mathbf{E}$ ). The other is negative dielectric anisotropy, in which  $\epsilon_{\perp}$  is larger than  $\epsilon_{//}$ . In addition, LCs in the  $N_F$  state show great sensitivity to electric fields due to their high dielectric permittivity ( $\epsilon > 10^4$ ).<sup>[40d]</sup> Different from the NLCs,  $N_F$ LCs show uniaxial polar ordering and alternating electric polarization exists with 180° domain walls. Basnet et al.<sup>[40a]</sup> demonstrated that in the  $N_F$  state, the applied electric field  $\mathbf{E} = E(0,1,0)$  of an amplitude of  $(1-10) \text{ kV m}^{-1}$ , along with the polarization  $\mathbf{P} = P(0,1,0)$ , did not cause textural changes in the conditions of 1–2  $\mu\text{m}$  thick LC cells. When  $\mathbf{E}$  is antiparallel to  $\mathbf{P}$ , above the critical field ( $-11 \text{ kV m}^{-1}$ ), the polarization is broken, which is parallel to  $\mathbf{E}$ . In addition, the CLC structure is the focus of electrical tunability. There are two types of electrical modifications of helicoidal CLCs: tuning the helicoid pitch<sup>[51b,52]</sup> and realigning the helicoid axis.<sup>[51a]</sup> Similar to the NLCs, when the CLCs are of negative dielectric, the alignment direction of LC molecules is vertical to  $\mathbf{E}$ , and due to a lack of torque, the pitch does not change. For positive dielectric anisotropy, the helical axis can be realigned perpendicular to  $\mathbf{E}$ . Besides the amplitude of the electric field, the frequency impacts the LC structure. Typically, dual-frequency LCs (DFLCs) can exhibit a positive dielectric anisotropy ( $\Delta\epsilon > 0$ ) in the low-frequency region and a negative dielectric ( $\Delta\epsilon < 0$ ) in the high-frequency region.<sup>[17d,51d]</sup> Furthermore, in the crossover frequency,  $\Delta\epsilon$  equals to zero. Moreover, the dielectric heating effect emerges as the oscillation of electrons under a high frequency, which helps to tune the CLCs' helicoid pitches considerably.<sup>[40c,51b]</sup> Furthermore, new research has demonstrated that the frequency-dependent photonic bandgap (PBG) in a wide spectral range happens in the heliconical CLCs system. Liu et al.<sup>[34a]</sup> investigated a dynamic helicoid architecture by mixing a positive dielectric LC mixture of E7 and the dimer CB7CB. The coupling and competition between the elastic effects and dielectric torque formed a heliconical structure. By tuning the frequency, the reflection spectrum can shift from 460 nm to nearly 1000 nm with a reversible transformation (Figure 3a).

The electric-induced LC structure change makes active optical applications versatile and outstanding. Introducing an external electrical field will lead to the realignment of LC molecules, and the optical performance will change greatly. Applying a DC voltage to polymer-stabilized CLCs with negative dielectric anisotropy will result in anion accumulating on the anode and cation located on the polymer, respectively, which leads to a mechanical force on the polymer network and an expanded and contracted gradient pitch length.<sup>[53]</sup> Moreover, by employing external voltages, tunable and multifunctional LC holography can be realized.<sup>[51c]</sup> Interestingly, by integrating LCD technology and plasmonic structural colors, Franklin et al.<sup>[17f,54]</sup> proposed a



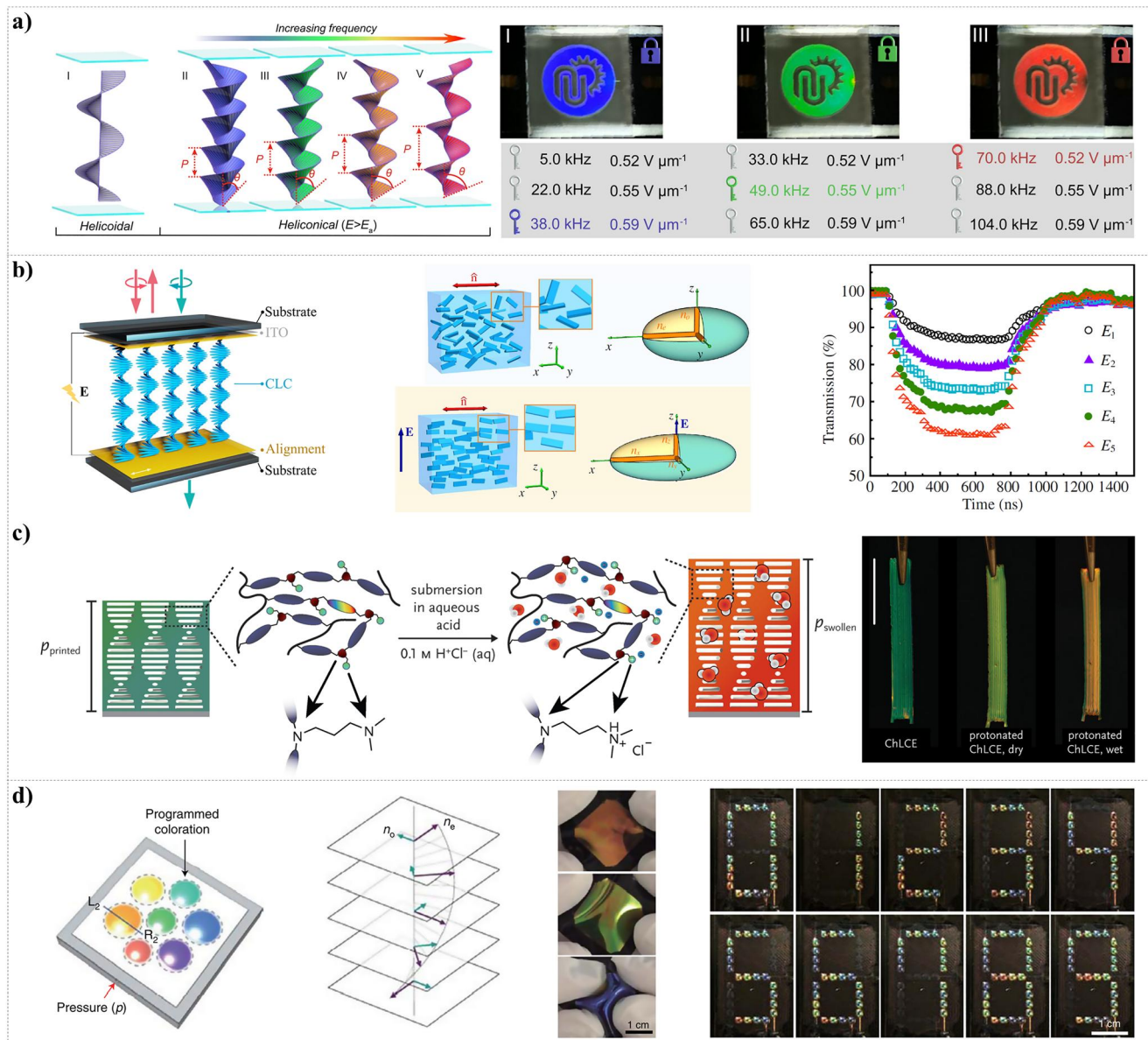


**FIGURE 3** LCs structure changes and dynamic performances under external electric field, humid, and mechanical force stimuli, respectively. (a) Frequency-actuated heliconical soft architecture and active information encryption. Reproduced with permission.<sup>[34a]</sup> Copyright 2022, Springer Nature. (b) Submicrosecond electro-optic switch of CLCs. Reproduced with permission.<sup>[34b]</sup> Copyright 2022, SPIE and CLP. (c) CLCE with acid treatment induced concurrent change in the cholesteric pitch length. Scale bar: 1 cm. Reproduced with permission.<sup>[56a]</sup> Copyright 2022, John Wiley and Sons. (d) The active structural coloration of a CLCE membrane induced by in-plane strain upon an arbitrary out-of-plane deformation. Scale bar: 1 cm. Reproduced with permission.<sup>[34c]</sup> Copyright 2022, Springer Nature. CLCE, cholesteric LCE; CLCs, cholesteric LCs; LCs, liquid crystals.

reflective hybrid display. In their work, the optimized LC layer played the role of tuning the polarization of incident light when the voltage was off; thus, the light could be reflected through the whole device, and the light could not get reflected when the voltage was on.<sup>[54]</sup> For the DFLC, its unique features to frequency can enable CLCs with multiple applications. CLCs suffer from a planar state, focal conic state, and vertically aligned state with distinct intensity and frequency of electric field, which help tune the polarization of light.<sup>[51d]</sup> For example, switching the voltages (46 V, 1 kHz, and 30 V, 50 kHz, respectively) caused the DFLC polarization volume grating to show a homeotropic and planar state,

respectively.<sup>[17d]</sup> The turn-on and turn-off response time of the grating was measured to be 11.55 and 1.36 ms, respectively. To achieve rapid electro-optic switching in soft photonic structures, Ma et al.<sup>[34b]</sup> demonstrated a shift of PBG of the order of 100 ns, relying on the mechanism that the electric fields modify the orientational order of molecules and quench their fluctuations, rather than altering the orientation (Figure 3b). Additionally, in the smectic A phase, TFCDs can be formed in the hybrid alignment condition. Different from common TFCDs, Wu et al.<sup>[51e]</sup> designed electrically tunable microlens TFCD arrays with polymer-stabilized SmA LC, whose focal length could be tuned with an electrical field.

## 2.4 | Other stimuli-responsive LCs

Humid and mechanical stress can also be applied to tune the structure of the LC system to change its optical performance, which is usually found in polymerized LC structures.<sup>[34e,55]</sup> Many commercial optical components, such as waveplates, are fabricated from NLC polymers. The CLC polymer (CLCP) can also perform active optical designs and applications, such as structural color and information encryption, where the helical pitch can be manipulated with humidity and mechanical stress.<sup>[34c,34e,56]</sup>

CLCPs, combining the optical features of CLCs and the elasticity of polymers, can reversibly tune their structure under humid stimuli after certain chemical operations. Sol et al.<sup>[56a]</sup> treated the cholesteric LCE (CLCE) with acid to make it respond to humidity. When exposed to water, the CLCE swelled and its volume changed, as a result, its reflected color changed simultaneously. The vibrant reflected spectrum shifted across the visible region when exposed to humid and dry air (Figure 3c). Additionally, Lan et al.<sup>[34e]</sup> successfully achieved cholesteric LCN (CLCN) structural color, where the reflected spectral color shifted from 460 to 625 nm as the relative humidity (RH) improved from 10% to 90%. By treating CLCN with a KOH solution, CLCN can also swell reversibly. Furthermore, by treating certain parts of CLCP film with  $\text{Ca}^{2+}$ , such as the heart-like region, the color of the CLCN pattern showed different color information under 10% and 90% RH, respectively. Thus, the novel information storage can be satisfied in this manner.

According to the mechanical stimulus, the soft LC structure can be tuned. Based on the large elasticity anisotropy and Poisson's ratio of CLCE, Kim et al.<sup>[34c]</sup> achieved a pixelated structural color with spectral color shifted from NIR to UV light. A shift in the spectrum was noted when the CLCE, positioned on poly(dimethylsiloxane) (PDMS) and embedded with air channels, experienced a change in the aspect ratio due to variations in the inflating region (Figure 3d). Pixelated coloration units can be established with spatial color dispersion, and cryptography can also be fulfilled by the pixelated coloration display. Hussain et al.<sup>[56b]</sup> demonstrated that the CLCE could be stretched with strain from 0% to 150%, and the wavelength of the photonic band gaps moved from 695 to 403 nm. Besides, the stretched CLCE reflected both right- and left-handed polarized light at the same time. By mechanical stretching, controlling multicolor switching enriches the application for disguising and information encryption.<sup>[56d]</sup>

## 3 | STIMULI-RESPONSIVE SILK PROTEINS

Naturally derived biomaterials (such as silk protein, cellulose, chitin, keratin, guanine, DNA, and natural pigments) are promising candidates for the development of sustainable optical platforms.<sup>[57]</sup> Biomaterials provide new opportunities for replacing existing nonrenewable optical platforms with

renewable, biocompatible, and biodegradable systems that match the high performance of their synthetic counterparts while minimizing waste, environmental degradation, and energy-intensive input. In addition, the features of hierarchical and tailorable structures, stimuli-responsiveness, functionalized capabilities, and facilitation of forming different soft material formats make them ideal for soft, smart, and stimuli-responsive optical materials. Silk protein stands out among the most extensively researched biopolymers due to its aptitude for forming diverse optical architectures. These generate an optical response resulting from the interaction of light with the micro-/nanostructures in which the silk protein is configured.<sup>[33c,58]</sup> Silk protein is a natural structural protein that is mainly spun by spiders and silkworms. Among the different sources, domestic *B. mori* silk is of the most interest for versatile applications owing to its availability in large quantities, along with its outstanding material characteristics. Silk proteins show multiple molecular responses under external stimuli, such as controllable polymorphic transition,<sup>[6c,59]</sup> reversible volume swelling and shrinking,<sup>[60]</sup> and programmable biodegradability,<sup>[23,61]</sup> making it a favorable platform for active optics. Over the past few decades, remarkable progress has been achieved in designing and producing dynamic, tunable optical micro/nanostructures by employing hierarchical manufacturing techniques for silk proteins.<sup>[62]</sup> This approach has led to the development of a wide range of optical materials and devices capable of responding to various external stimuli, including chemical species, temperature, light, and mechanical strain. These responsive optical systems appeal greatly to many high-tech applications, including smart displays, information processing, soft actuators, and bio-interfaces.<sup>[58,63]</sup> In this section, we summarize state-of-the-art dynamically responsive optical systems that have been constructed using silk proteins as key building materials.

## 3.1 | Chemically responsive silks

Chemically responsive silk optical platforms can be achieved through the swelling and shrinking of the silk matrix in response to external stimuli from various chemical species. This dynamic behavior is driven by specific physical or chemical bonding interactions between the optical substrates and chemicals involved, including humidity/vapors, solvents, and pH variations. The inherent responsiveness of these optical platforms enables adjustment of their macro-scale characteristics, such as structural color and transparency, in response to specific chemical stimuli.

Amorphous silk protein undergoes a controllable and irreversible transition between polymorphic structures in response to water vapor.<sup>[64]</sup> The essence of silk conformational transitions lies in the molecular movement at the nanoscale, creating reconfigurable silk-based photonic systems. Large-scale and reconfigurable silk photonic films, including silk inverse opals (SIOs), photonic crystal superlattices, and hierarchical opals, have recently been developed



by leveraging the polymorphic transition of silk proteins. Wang et al.<sup>[65]</sup> found that these amorphous silk photonic structures are stable under ambient conditions; however, upon exposure to water vapor, the photonic lattice can be controllably compressed along the vertical direction of the film, resulting in the reconfiguration of the PBG. This mechanism allows for tuning of the macroscale structural color over the entire visible spectrum.

With the aid of shadow masks, multicolor patterns can be easily generated by selectively exposing masked silk photonic films to water vapor for various durations (Figure 4a). Apart from water vapor, Li et al.<sup>[12a]</sup> proposed that solvents capable of inducing conformational transitions in silk proteins can be utilized to reconfigure photonic lattices. This capability was recently demonstrated by creating high-resolution patterned photonic crystals via inkjet printing, utilizing a mixture of methanol and water as ink components. The precise regulation of the ink composition or volume enables the attainment of diverse volumetric alterations within the silk matrix, thereby leading to distinct variations in the lattice constant and reflected colors (Figure 4b).

However, crystalline silk offers an ideal platform for generating reversible volume of swelling and shrinking in response to humidity/aqueous solvents because its molecular chains are anchored through physical crosslinking, allowing for the development of reversibly tunable photonic devices. A series of silk-based, dynamically responsive optical

platforms, ranging from inverse opals,<sup>[65]</sup> thin-films,<sup>[66]</sup> multilayer interference structures,<sup>[60]</sup> optical fibers,<sup>[67]</sup> metal-insulator-metal resonators,<sup>[68]</sup> plasmonic devices,<sup>[69]</sup> to metamaterials,<sup>[70]</sup> have been developed. The high sensitivity of the crystalline silk matrix to humidity renders these silk-based optical devices suitable for sensing applications.

By integrating optical elements into pH-responsive silk materials, it is possible to alter the macroscopic visual characteristics, such as structural colors, of the resulting platform in response to changes in pH levels. Cheng et al.<sup>[71]</sup> developed an intelligent spider silk protein textile with a tunable structural color by embedding a microfluidic channel compounded with a pH-responsive photonic crystal structure. The surfaces of synthetic photonic crystals can exhibit a substantial aggregation of the carboxyl groups and amino groups. As a result, the photonic crystal film displays responsiveness to hydrogen or hydroxyl ions present in an aqueous solution and demonstrates a structural color that is dependent on pH. Incorporating a photonic crystal elastic film in this pH-responsive textile makes it suitable for pH monitoring in wound-management applications.

### 3.2 | Thermoresponsive silks

Silk proteins can be used individually or in combination with other materials to construct thermoresponsive optical

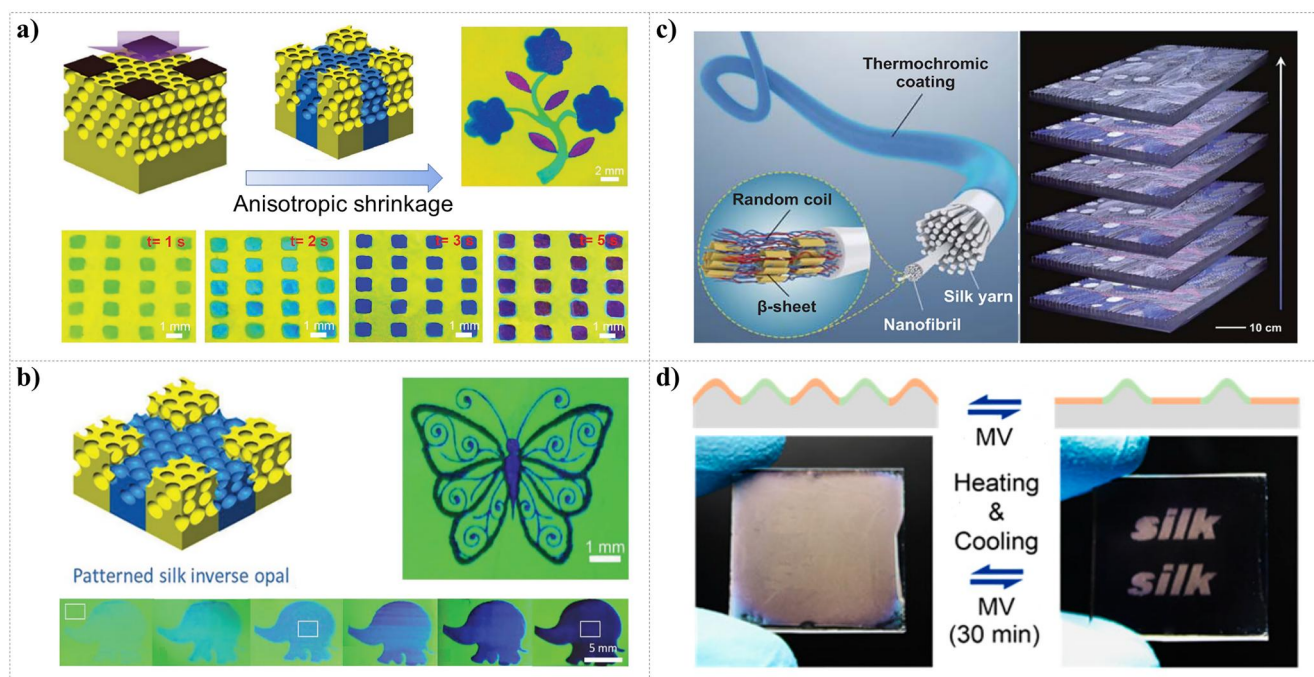


**FIGURE 4** Chemically and thermally sensitive silks for optical platforms. (a) Patterned SIOs are formed using a shadow mask (up). Scale bars: 2 mm; photographs of patterned SIOs by water-vapor treatment (bottom). Scale bars: 1 mm. Reproduced with permission.<sup>[65]</sup> Copyright 2017, John Wiley and Sons. (b) Schematic diagram of patterned SIO and cartoon elephants with different colors on 10-layer-SIO films by changing MeOH/water composition. Scale bars: 1 mm (up); scale bars: 5 mm (bottom). Reproduced with permission.<sup>[12a]</sup> Copyright 2019, John Wiley and Sons. (c) Schematic illustration of the hierarchical interfaces in TCS fibers; photographs of color-changing TCS weaving pattern when the heat source passed from left to right. Scale bars: 10 cm. Reproduced with permission.<sup>[72]</sup> Copyright 2021, Springer Nature. (d) Schematics (top) and photographs (bottom) of switching between the pattern display and hiding process. Reproduced with permission.<sup>[74]</sup> Copyright 2019, National Academy of Sciences. SIO, silk inverse opal; TCS, thermochromic silk.

platforms. Thermally responsive optical devices based solely on silk proteins rely on large negative thermal expansion coefficients. For example, silk fibroin-based, temperature-responsive whispering gallery microresonators showed a significant resonant wavelength shift as a function of temperature, making them suitable for high-precision thermal sensors.<sup>[22a]</sup> By incorporating thermoresponsive components with silk proteins, this platform can achieve various dynamic and tunable optical functionalities. The introduced components may exhibit heat-induced phase transitions or swelling–deswelling abilities under temperature fluctuations. For instance, Wang et al.<sup>[72]</sup> (Figure 4c) developed a low-cost and effective strategy to produce thermochromic silks (TCSs) by combining yarn spinning and continuous dip-coating techniques. The resulting TCSs exhibited programmable thermochromic responses with excellent cyclic stability. Zheng et al.<sup>[73]</sup> prepared a nanocomposite for temperature sensing by combining a hydrogel composed of silk fibroin and poly-*N*-isopropyl acrylamide with a colloidal photonic crystal template. The composite photonic structure undergoes shrinkage or relaxation in response to temperature changes, resulting in a variation in structural colors ranging from blue to orange-red. This characteristic holds the potential for real-time monitoring of dynamic human temperature changes.

Combining thermally responsive behaviors with the polymorphic transition of silk proteins also allows for the acquisition of switchable optical functions. To demonstrate this, Wang et al.<sup>[74]</sup> fabricated reversible and dynamic wrinkled micropatterns. In this scenario, a bilayer system composed of a silk film layer with a higher Young's modulus and a PDMS substrate with a lower Young's modulus were subjected to thermal stimuli, and a wrinkle pattern emerged after cooling because of the mechanical mismatch between these two materials. The wrinkled surfaces are stable under ambient conditions but can be erased when exposed to external stimuli (such as water vapor, methanol vapor, or UV light) because of the induced molecular rearrangement of silk fibroin and thus the release of compressive stress within the system. The reversible transition between the wrinkled and wrinkle-free states leads to switchable optical transparency. As such, the patterns underneath the device could be reversibly displayed (Figure 4d). In addition, wrinkling systems can be combined with other top-down transformation approaches, such as the mask method, inkjet printing, and fingerprinting, to create patterned wrinkling surfaces for information storage, encryption, and security.

### 3.3 | Phototunable silks

Using light with a precise wavelength capable of inducing a controlled glass/conformational transition of silk proteins presents another crucial approach for creating phototunable optical platforms. Deep UV light with a wavelength of 254 nm has been demonstrated to be an effective stimulus for redefining silk optical structures because of its unique

capability to induce peptide chain scission and photo-degradation of silk protein.<sup>[64a]</sup> Mid-infrared light can induce the glass/polymorphism transition of silk proteins, and Lee et al.<sup>[6b]</sup> developed a rewritable optical storage medium by leveraging tip-enhanced near-field infrared nanolithography. Such a technique can induce controlled topographical and/or structural changes in silk protein, enabling the reversible formation of high-density nanodot arrays with a spatial resolution of ~35 nm and a 100 nm feature size of pattern spacing (Figure 5a). The authors demonstrated that such silk drives exhibit high digital and biological information (by doping with biological dopants) storage capacity (~64 GB inch<sup>-2</sup>) and long-term stability under various harsh conditions, benefiting from the excellent material properties of silk protein.

Optical multiplexing technology, which exploits the spatial characteristics of light, such as angle, amplitude, phase, and polarization, as distinct information channels to encode independent information, has emerged as a compelling approach for achieving color image transformation. Wang et al.<sup>[75]</sup> recently demonstrated that angle-induced reversible pattern switching could be accomplished by creating silk photonic films featuring asymmetric multicolor patterns. The photonic film was generated by integrating surface plasmon resonance (SPR) and PBG effects in a single material. The dominant control of the color appearance by SPR on one side of the film and the PBG effect on the other side allows for the display of different multispectral pattern designs on each side of the film (Figure 5b). More interestingly, by simply tuning the relative contributions of SPR and PBG effects through the modulation of light irradiation/viewing angle, this photonic composite film showed the possibility of reversible pattern displays, opening new paths toward double-sided display applications, such as smart visual indicators or warning signs.

Incorporating a photosensitive material or dye into a silk matrix offers another straightforward strategy for modulating its optical characteristics in response to light stimuli. Photonic crystal structures that can control light flow by strongly suppressing the propagation of photons of specific frequencies through the structure can be used as light-harvesting layers in various optical devices to enhance light-energy conversion.<sup>[76]</sup> Wang et al.<sup>[77]</sup> recently utilized this strategy to develop photonic actuators, in which embedded photonic structures can act as light-reflecting layers to manipulate the energy conversion from optical energy to mechanical action. By integrating SIO films with elastomeric materials (Figure 5c), the developed optomechanical devices could achieve controllable and tunable actuation and complex deformation in response to simple light illumination. The ability to program the PBG through photonic lattice modification enables the generation of complex three-dimensional (3D) configurations and different motion modes. Phototropic movement, in which the material moves in response to the motion of a light source, can be realized by harnessing the angular dependence of the PBG. This was demonstrated by creating a “photonic sunflower”,

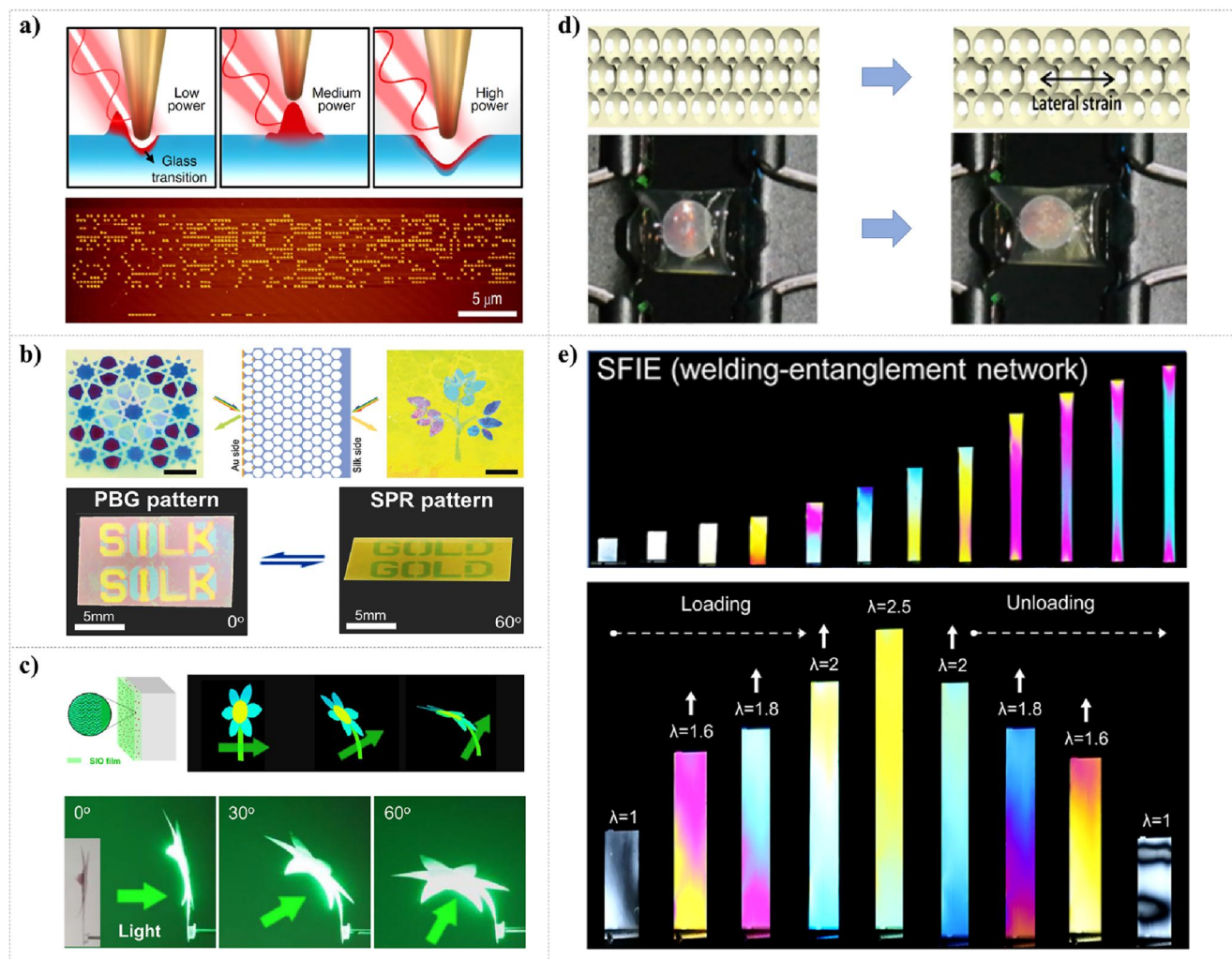


**FIGURE 5** Light and mechanical stress-induced structural change and application of silks. (a) Schematics of three types of responses of silk thin film to applied laser powers; example of a silk drive. Scale bars: 5  $\mu\text{m}$ . Reproduced with permission.<sup>[6b]</sup> Copyright 2020, Springer Nature. (b) Asymmetric multicolor pattern viewed from the Au and silk sides; switching between PBG and SPR patterns. Scale bars: 5 mm. Reproduced with permission.<sup>[75]</sup> Copyright 2022, John Wiley and Sons. (c) Structure schematic and photograph of a bilayer photonic sunflower; schematics and photographs of different deformation states of the photonic sunflower responding to different illumination angles. Reproduced with permission.<sup>[77]</sup> Copyright 2021, Springer Nature. (d) Schematics and photographs of silk hydrogel inverse opal before and after stretching. Reproduced with permission.<sup>[22b]</sup> Copyright 2017, National Academy of Sciences. (e) Polarized images of SFIE during tensile testing; polarized images of the SFIE during stretching and recovery. Reproduced with permission.<sup>[79]</sup> Copyright 2023, American Chemical Society. PBG, photonic bandgap; SFIE, silk fibroin ionoelastomer; SPR, surface plasmon resonance.

in which the petals and stamens keep facing the light due to the continuous bending of the pedicel. This phototropic system was used as a light-tracking device to enhance the light-to-energy conversion efficiency of the loaded solar cells. The solar cells track the light source continuously as the light source moves, thereby dramatically maximizing efficiency. Apart from simple solution mixing, introducing optical functionality into silk-based materials can be achieved through chemical modification of silk protein, exploiting its abundant surface chemistry. In this context, a prevalent approach involves the incorporation of azobenzene moieties into silk structures, leading to the development of a photoresponsive biomaterial known as azosilk.<sup>[78]</sup> This platform exhibits tunable optical absorption through

reversible photoswitching between the *trans* and *cis* geometric isomers of azobenzene molecules.

### 3.4 | Mechanochromic silks

Silk materials are also capable of reversibly responding to mechanical strain. Mechanically responsive tunable optics can be realized by continuous and reversible variations in optical structures in response to the tensile stress applied to them. Therefore, such optical platforms are typically used for strain sensing, in which silk hydrogels provide an ideal material format for transforming a mechanical stimulus into an optical signal. Min et al.<sup>[22b]</sup> presented a deformable and



conformal silk hydrogel inverse opal as a typical example. The elastic deformation of the hydrogel induced an anisotropic change in the photonic lattice constant of the SIO, leading to a reversible adjustment of the reflected structural color (Figure 5d). Zhang et al.<sup>[79]</sup> developed a novel type of silk fibroin ionoelastomer (SFIE) that exhibits exceptional stretchability and minimal hysteresis by incorporating dimension-and-content-confined nanocrystalline crosslinks into amorphous and molecularly entangled silk fibroin ionotronics (SFI) (Figure 5e). These SFIE materials not only displayed improved stretchability but also exhibited a gradual enhancement in birefringence as they were subjected to stretching. Furthermore, the SFIE materials demonstrated vibrant interference colors in comparison with their SFI counterparts, and these colors exhibited reversible changes from pink to yellow when subjected to stretching and subsequent recovery. The remarkable mechanochromic properties of SFIEs make them highly promising optical materials for various applications, including human-machine interfaces and bio-functional devices.

## 4 | STIMULI-TUNABLE LUMINESCENT MATERIALS

The responsive materials mentioned above are optically inert, which can modulate the incident light through the optical structure but cannot emit light. Recently, luminescent materials have been studied extensively as responsive materials. Here, we would like to select lanthanide ( $\text{Ln}^{3+}$ )-based luminescent materials as representatives because of their excellent optical properties, diverse application scenarios, and most importantly, responsiveness to multiple stimuli. Both the downshifting luminescence (DSL) and upconversion luminescence (UCL) of  $\text{Ln}^{3+}$  comprise the following steps: (1) pumping of excited states, (2) non-radiative relaxation, (3) radiative transitions, and (4) a ubiquitous energy transfer process between excited states with similar energy level positions.<sup>[26e,80]</sup> These steps are associated with the energy level structure and coordination environment of  $\text{Ln}^{3+}$ . Therefore, as long as the external stimuli influence the above factors, the overall luminescent properties will respond correspondingly, which are the basis for realizing in situ and reversible optical regulation.

In Section 4, we focus on the responsive behavior of luminescent materials to physical stimuli and introduce strategies for luminescence modification based on stimuli, such as heat, light, electric field, magnetic field, and mechanical stress, which are widely utilized to regulate luminescent properties.

### 4.1 | Heat-modulated luminescence

As a fundamental physical parameter, temperature affects every part of the luminescent system. First, the excited energy levels of  $\text{Ln}^{3+}$  may respond differently to temperature

changes, resulting in variations in the emission intensity ratio at different temperatures. As a representative example, the  $^2\text{H}_{11/2}$  and  $^4\text{S}_{3/2}$  levels of  $\text{Er}^{3+}$  ions are thermally coupled because of the small energy gap between them. As the temperature increases, the population of excited electrons follows the Boltzmann distribution, which means that the electrons tend to be populated at a higher  $^2\text{H}_{11/2}$  energy level instead of a lower  $^4\text{S}_{3/2}$ . This behavior leads to a temperature-dependent intensity ratio of emission from  $^2\text{H}_{11/2}$  and  $^4\text{S}_{3/2}$  and establishes the foundation for  $\text{Er}^{3+}$ -based ratiometric luminescent thermometry.<sup>[85]</sup>

Second, the emission intensity is always dependent on the ambient temperature. High temperatures are generally considered to be deleterious for lanthanide-based luminescent materials, in which the excitation energy largely dissipates via enhanced non-radiative transition at high temperatures.<sup>[86]</sup> This so-called thermal quenching (TQ) luminescence severely limits the applications of lanthanide luminescence. Fortunately, in the past decades, researchers have found that increasing the surrounding temperature can also modify the interionic distance and crystal field symmetry of the host lattice, resulting in abnormal luminescence enhancement.<sup>[87]</sup> Moreover, thermal-induced desorption of surface moisture and surface phonon-assisted energy transfer were employed to explain thermally enhanced UCL of lanthanide-doped nanocrystals.<sup>[88]</sup>

In addition, heat-triggered energy compensation from the energy trapper in the host lattice to activators is a feasible mechanism for realizing thermally enhanced luminescence of various activators, including  $\text{Yb}^{3+}$ ,  $\text{Er}^{3+}$ ,  $\text{Eu}^{2+}/\text{Eu}^{3+}$ ,  $\text{Tb}^{3+}$ ,  $\text{Sm}^{3+}$ ,  $\text{Pr}^{3+}$ ,  $\text{Cr}^{3+}$ , etc.<sup>[81,89]</sup> Wei et al.<sup>[81]</sup> reported Frenkel defect-modulated thermally enhanced lanthanide luminescence in  $\text{Sc}_2(\text{WO}_4)_3:\text{Ln}$  phosphor. Upon heating, the distortion of partial  $\text{WO}_4^{2-}$  from intrinsic to extrinsic positions in  $\text{Sc}_2(\text{WO}_4)_3:\text{Ln}$  forms the Frenkel defect, which acts as an energy reservoir and compensates the energy depletion of  $\text{Ln}^{3+}$  due to TQ through the back-transfer of stored energy to  $\text{Ln}^{3+}$  (Figure 6a). Thus, thermally enhanced DSL and UCL of  $\text{Ln}^{3+}$  was realized in  $\text{Sc}_2(\text{WO}_4)_3:\text{Ln}$ . Moreover, they demonstrated that the prominent negative thermal expansion feature of the host only contributes ~2% to the enhancement and that the thermally enhanced luminescence is highly promising for solar energy harvesting by integrating  $\text{Sc}_2(\text{WO}_4)_3:\text{Ln}$  with a thermophotovoltaic cell.

### 4.2 | Light-altered luminescence

The parameters of the excitation light of luminescent materials, including the excitation wavelength, excitation power density, excitation pulse width, and polarization angle, determine the overall performance of luminescence, which is a widely employed toolbox for luminescence regulation.

For luminescent materials with a single optical center, the excitation and emission peaks are usually fixed because only one set of ground and excited energy levels exist. When other optical centers are introduced through multiple ion

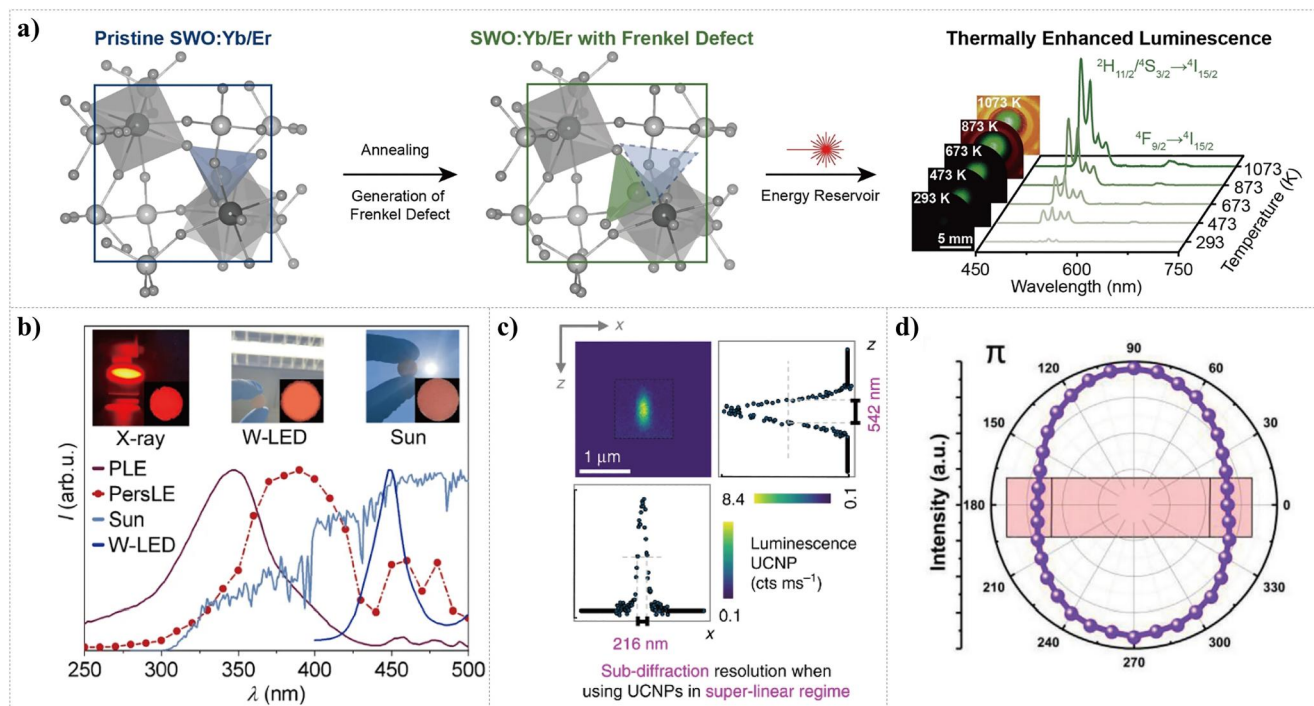


**FIGURE 6** Responsive behaviors of luminescent materials to heat and light stimuli. (a) Illustration of Frenkel defect-modulated lanthanide luminescence in  $\text{Sc}_2(\text{WO}_4)_3:\text{Ln}$ . Reproduced with permission.<sup>[81]</sup> 2023, John Wiley and Sons. (b) Comparison of white light emitting diode emission spectra, solar spectra, excitation spectra, and PersL of  $\text{NaGdTi}_2\text{O}_6:0.1\%\text{Pr}^{3+}$  at room temperature. Reproduced with permission.<sup>[82]</sup> 2022, Nature Springer. (c) The resolution of super-resolution techniques at high power density. Reproduced with permission.<sup>[83]</sup> 2019, Nature Springer. (d) Polar plots of upconversion emission intensity at 483 nm of  $\beta\text{-NaYF}_4:20\%\text{Yb}^{3+}, 10\%\text{Pr}^{3+}$  microcrystals as a function of excitation polarization angle. Reproduced with permission.<sup>[84]</sup> 2019, John Wiley and Sons. PersL, persistent luminescence.

doping,<sup>[90]</sup> selective reduction,<sup>[91]</sup> or defect engineering,<sup>[82]</sup> the overlapped excitation bands of different optical centers and the energy transfer between them will lead to excitation wavelength-dependent luminescence, which show the variation of both emission intensity and peak position.

For example,  $\text{Er}^{3+}$ -based multilayer core-shell nanoparticles show a color-switchable output under irradiation with 808, 980, and 1535 nm light.<sup>[92]</sup> Each excitation wavelength may trigger a different UCL process, which results in a tunable emission color and has potential applications in data storage and information decoding. Zhou et al.<sup>[82]</sup> further reported an excellent luminescent phosphor (Figure 6b),  $\text{NaGdTi}_2\text{O}_6:\text{Pr}^{3+}/\text{Er}^{3+}$ , that possesses long persistent luminescence, DSL, and UCL from doped  $\text{Ln}^{3+}$  and defect levels. Under the excitation from X-rays to sunlight, switching off the luminescence process in  $\text{NaGdTi}_2\text{O}_6:\text{Pr}^{3+}/\text{Er}^{3+}$  shows intense colorful luminescence statically and dynamically, which is utilized for multilevel anti-counterfeiting.

The power density is another basic parameter of steady-state light excitation. For emissions involving a single-wavelength excitation, such as the DSL of  $\text{Ln}^{3+}$ , a facile way to alter the emission intensity is to change the excitation power density because a higher power density usually results in stronger emission. However, regarding nonlinear UCL, different UCL processes usually exhibit disparate responses to the power density.<sup>[93]</sup> Generally, high-order UCL requires

more excitation photons. Thus, the radiative transition from high-lying levels is only possible under a high excitation power density. Therefore, a high power density is desirable for realizing bright and multiphoton UCL. For instance, the super-linear change in the UCL, as the power density increases, can be utilized to improve the performance of super-resolution techniques (Figure 6c).<sup>[83]</sup>

Unlike steady-state UCL under the excitation of continuous-wave lasers, nonsteady-state excitations with different pulse widths and frequencies can dynamically modulate the emission color. This responsive behavior arises from the different luminescence decay rates of excited states.<sup>[94]</sup> Fu et al.<sup>[95]</sup> reported that photons depopulated from the red emissive energy level can be excited again by the next pulse excitation, which does not occur for the green energy state. Therefore, they can dynamically control the emission color by adjusting the excitation frequency and constructing a three-dimensional encryption application. Yang et al.<sup>[29b]</sup> reported a strategy to obtain switchable NIR emission of upconversion nanoparticles (UCNPs) at 800 nm by modulating the excitation pulse width and realized orthogonal activation of in vivo photoacoustic imaging and photodynamic therapy through the combination of steady and nonsteady state excitation.

The response of the emission intensity to the excitation polarization angle is another fascinating feature of lanthanide luminescence. Owing to the anisotropic photoelectric

properties of  $\text{Ln}^{3+}$ , the emission intensity changes as the polarization angle of the excited light changes. Yang et al.<sup>[84]</sup> used density functional theory calculations and carefully controlled experiments to explain the anisotropic excitation polarization response for the first time. They demonstrated that the  $\text{F}^-$  ion distribution difference determines the polarization properties of the  $\beta\text{-NaYF}_4\text{:Yb/Er}$  microcrystals. As seen from the *c*-axis of the crystal lattice, the  $\text{F}^-$  ions are distributed uniformly and lead to no excitation–polarization dependence. In contrast, the  $\text{F}^-$  ions are distributed inhomogeneously around  $\text{Ln}^{3+}$  ions when seen from the direction perpendicular to the *c*-axis; therefore, an obvious periodical change of UCL intensity is observed when the excitation polarization angle varies from  $0^\circ$  to  $360^\circ$  (Figure 6d). Moreover, such polarized lanthanide luminescence can be realized and extended to the macroscale through the ordered assembly of anisotropic luminescent nanomaterials.<sup>[96]</sup>

### 4.3 | Electric field-tuned luminescence

An electric field is a widely used control method to regulate the physical and chemical properties of functional materials. For lanthanide luminescence, electronic transitions within the 4f orbit of  $\text{Ln}^{3+}$  are shielded by the outer 5s/5p orbitals; therefore, these electronic transitions are hardly responsive to the applied electric field.<sup>[26a]</sup> However, electronic transitions are sensitive to changes in host lattice-related parameters, such as crystal structure and local site symmetry. This paves the way for manipulating lanthanide luminescence by controlling the host lattice using an applied electric field.<sup>[101]</sup>

For example, dielectric hosts such as ferroelectric materials can be polarized by an external electric field, under which circumstances the cations or anions in the ferroelectric lattice deviate along or against the direction of the electric field, respectively. This leads to distortion of the crystal structure and breakdown of the local site symmetry. Generally, a lower local site symmetry favors stronger emission of  $\text{Ln}^{3+}$  because of the larger probability of radiative transitions.<sup>[102]</sup>

Hao et al.<sup>[97]</sup> first reported electric-field-mediated UCL tuning of  $\text{Er}^{3+}$  in ferroelectric  $\text{BaTiO}_3\text{:Yb/Er}$ . They built a heterostructure device consisting of a  $\text{BaTiO}_3\text{:Yb/Er}$  film deposited on a conductive  $\text{SrRuO}_3$ -coated  $\text{SrTiO}_3$  substrate and monitored the luminescence at various electric fields (Figure 7a). Under an external electric field, a slight displacement of  $\text{Ti}^{4+}$  and  $\text{O}^{2-}$  toward opposite directions occurs and reduces the crystal field symmetry around  $\text{Er}^{3+}$ , which leads to enhanced emission. The overall green emission intensity from  $^2\text{H}_{11/2}/^4\text{S}_{3/2} \rightarrow ^4\text{I}_{15/2}$  of  $\text{Er}^{3+}$  was enhanced 2.7 times under a voltage of 10 V, while the red emission remained unchanged. The different responsive behaviors of red and green emissions come from the different sensitivities of their radiative transitions to changes in the local site symmetry. Thus, both tunable luminescence intensity and red/green intensity ratio were achieved. Similarly, the enhanced DSL of  $\text{Eu}^{3+}$  was realized by the electric field in the  $\text{BaTiO}_3$ -based lead-free piezoceramic.<sup>[103]</sup>

In addition, electrically modulated lanthanide luminescence can be realized in hybrid luminescent materials comprising UCNP and electrochemically responsive organic molecules (Figure 7b). Inspired by electrochromic organic molecules for optoelectronic applications, Wu et al.<sup>[98]</sup> reported dynamic modulation of UCL color and intensity based on molecular-assisted surface electrochemical tuning. Under an applied external electric field, the oxidized and reduced states of viologen molecules can be easily switched by controlling the electric field direction, which leads to electrically controlled energy transfer from the UCNP to the molecules, thereby resulting in different emission colors. They further constructed a programmable logic gate array to convert the information-encrypted electrical signals into visible patterns.

### 4.4 | Magnetic field-tuned luminescence

The interaction between the magnetic field and optical properties, that is, magneto–optic interactions, has been widely studied and utilized to regulate the luminescence profiles of various luminescent materials. For lanthanide luminescence, the energy level structure of  $\text{Ln}^{3+}$  and the host lattice are sensitive to an external magnetic field, which influences luminescence properties. Although the underlying mechanism of the magneto–optic interaction is not fully understood, it is widely accepted that the magnetic field-induced Zeeman splitting of energy levels is the main reason for the magnetic-responsive luminescence properties of lanthanide ions.<sup>[101]</sup>

As shown in Figure 7c, tunable luminescence of  $\text{Er}^{3+}$  by an external magnetic field was observed early in  $\text{PbF}_2\text{:Er}$  and  $\text{NaGdF}_4\text{:Nd/Yb/Er}$  nanocrystals, which was caused by the splitting of the energy levels of  $\text{Er}^{3+}$  at an increased magnetic field.<sup>[99,104]</sup> Specifically, when a magnetic field is applied to  $\text{Er}^{3+}$ -doped luminescent materials, two doublets of the original  $^4\text{S}_{3/2}$  level are further split into four Zeeman levels  $|+1/2\rangle$ ,  $|-1/2\rangle$ ,  $|+3/2\rangle$ , and  $|-3/2\rangle$ . Subsequently, the energy gap between  $|-1/2\rangle$  and  $|-3/2\rangle$  increases with the magnetic field. Because the emission of the  $^4\text{S}_{3/2}$  level comes mainly from the lowest  $|-3/2\rangle$  level, and the lower levels always possess a lower probability of radiative transition, the emission intensity from the  $^4\text{S}_{3/2}$  level was suppressed by the increased magnetic field.

Beyond that, the magnetic field-induced Zeeman splitting increases the number of excited levels, which enhances cross-relaxation, and the lowering of the energy position of excited levels may reduce energy absorption abilities. Therefore, suppressed luminescence intensity was always observed, accompanied by spectral broadening and emission peak shift.<sup>[105]</sup> Even so, there are examples of magnetic field-induced luminescence enhancement.<sup>[106]</sup> For instance, when  $\text{Yb}^{3+}\text{--Er}^{3+}$  co-doped nanoparticles are considered, an external magnetic field can strengthen the energy transfer from  $\text{Yb}^{3+}$  to  $\text{Er}^{3+}$  as the magnetic field-induced Zeeman splitting reduces the energy difference



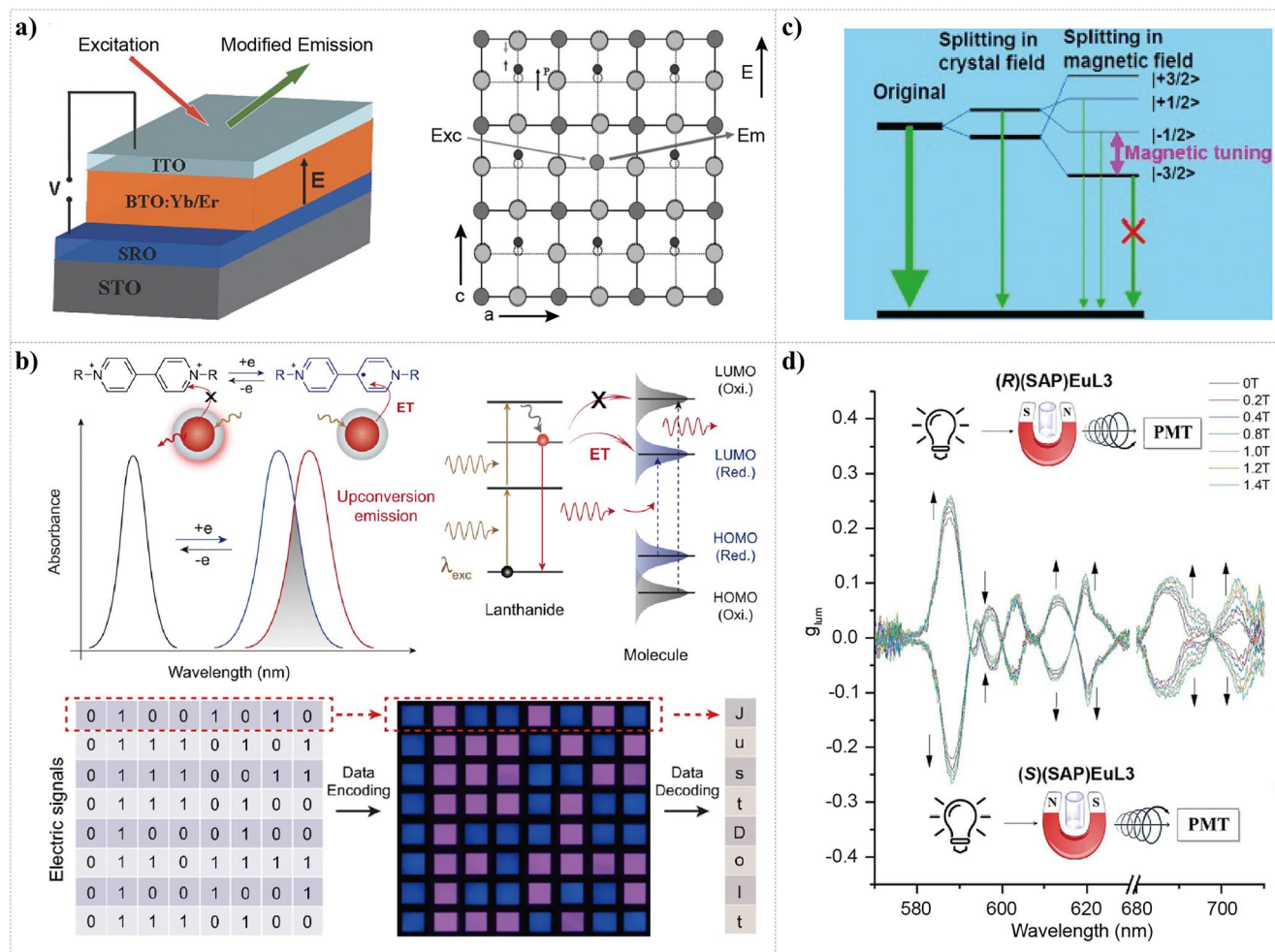


**FIGURE 7** Responsive behaviors of luminescent materials to electric and magnetic fields. (a) Illustration of the mechanism for the modulation of UCL under an external electric field. Reproduced with permission.<sup>[97]</sup> 2011, John Wiley and Sons. (b) MASET tuning and multiplexed data processing through opto-electrochemical modulation. Reproduced with permission.<sup>[98]</sup> 2021, Springer Nature. (c) Splitting  $4S_{3/2}$  energy level of  $Er^{3+}$  with an applied magnetic field. Reproduced with permission.<sup>[99]</sup> 2013, John Wiley and Sons. (d) Magnetic field-dependent  $g_{lum}$  spectra of (R)&(S)(SAP)EuL3 under 350 nm excitation at room temperature. Reproduced with permission.<sup>[100]</sup> 2020, John Wiley and Sons. MASET, molecular-assisted surface electrochemical tuning; UCL, upconversion luminescence.

between the excited states of  $Yb^{3+}$  and  $Er^{3+}$ , thus enhancing the emission intensity.

In addition to the modulation of the emission intensity and peak position, the polarization properties of lanthanide luminescence are tunable when a magnetic field is applied. For instance, Zhang et al.<sup>[100]</sup> introduced chiral substituents into macrocyclic scaffolds and achieved magnetic-responsive circularly polarized luminescence (CPL). As the external magnetic field increases from 0 to 1.4 T, the relaxation rates of the +M and -M Zeeman sublevels respond differently, leading to a net orientation of the emitting state. Thus, the  $g_{lum}$  values of  $^5D_0 \rightarrow ^7F_1$  transition of  $Eu^{3+}$  displayed a linear relationship and were enhanced by 20% from 0.222 to 0.267 (Figure 7d). This mechanism can be extended to other luminescent materials and provides an alternative for the fabrication of magnetically responsive optoelectronic devices.

## 4.5 | Mechanical stress-regulated luminescence

Mechanical stress is another important factor in the regulation of luminescence. By applying external stresses, such as contact forces, ambient press, or ultrasonic vibration, structural and chemical modifications of luminescent materials may occur, which is the underlying mechanism for mechanical stress-responsive luminescence modulation.

For lanthanide-based luminescent materials, high pressure is the most frequently used method, which brings forth variations that influence luminescent profiles, including shortened interionic distance, changes in crystal field, modification of emissive energy level, and even phase transformation. These factors can lead to the modulation of the emission intensity, peak position, and luminescence lifetime.

Second, it is worth noting that the emission of mechanoluminescent materials also responds to various stresses, which is promising for applications in luminescent sensors and artificial skin. Du et al.<sup>[107]</sup> developed a general method to incorporate a series of  $\text{Ln}^{3+}$  ions into  $\text{CaZnOS}$  to create multicolor mechanoluminescence emissions under mechanical excitations (Figure 8a), which demonstrates potential applications in optically encoded graphics for anti-counterfeiting.

Specifically, an external force can trigger the generation of polarization charges in the CaZnOS lattice, which produces a piezo potential inside the CaZnOS crystal and thereby tilts the valence and conduction bands. Under these conditions, the trapped electrons in CaZnOS are ejected to

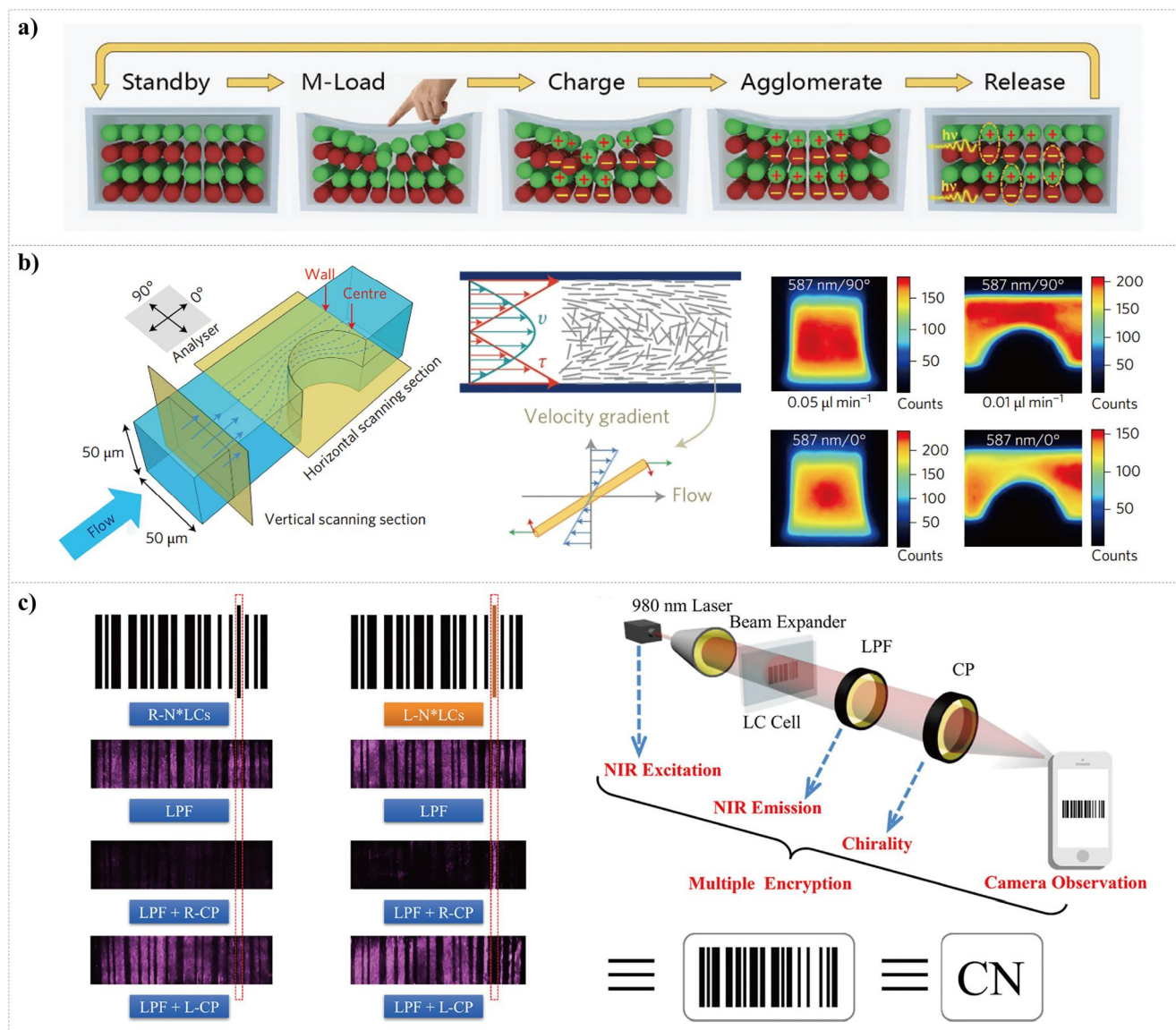


**FIGURE 8** Responsive behaviors of luminescent materials to mechanical stress stimulus and tunable luminescent materials combined with LCs. (a) Mechanism of ML in the CaZnOS: Ln. Reproduced with permission.<sup>[107]</sup> 2019, John Wiley and Sons. (b) Mechanism and illustration of the microfluidic channel used for the local shear rate measurement. Reproduced with permission.<sup>[29a]</sup> 2017, Springer Nature. (c) Photonic barcode and corresponding imaging setup based on the dually enhanced UC-CPL. Reproduced with permission.<sup>[108]</sup> 2023, American Chemical Society. LCs, liquid crystals; ML, mechanoluminescence; UC-CPL, CPL behavior based on the UCL of Ln<sup>3+</sup>.

the acceptor state and undergo recombination of the de-trapped electron and hole levels. Thus, the characteristic luminescence of doped  $\text{Ln}^{3+}$  ions can be sensitized by absorbing the released energy. This stress-triggered luminescence covers not only the emission peaks of  $\text{Tb}^{3+}$  from the violet to the red region but also the intrinsic defect emission around 490 nm and subsequently sensitized UCL from  $^5\text{D}_3$  energy levels of  $\text{Tb}^{3+}$ . Tu et al.<sup>[111]</sup> further illustrated the interaction between the ferroelectric properties and piezoluminescence intensity by investigating the real-time luminescent response of  $\text{Nd}^{3+}$  in the ferroelectric and paraelectric phases.

Unlike the works discussed above, in which physical modification is the main reason for luminescence regulation, luminescence modulation has recently been realized in  $\text{Tb}(\text{BTC})(\text{H}_2\text{O})_6$  metal–organic frameworks through pressure-induced chemical modification.<sup>[112]</sup> When treated by external pressure, enhanced hydrogen bonds allowed an optimized intersystem crossing process, which strengthened the energy transfer process from the triplet state to doped  $\text{Ln}^{3+}$ , thereby realizing an 8.6-fold luminescence enhancement of  $^5\text{D}_4$ – $^7\text{F}_5$  transition in  $\text{Tb}^{3+}$ .

#### 4.6 | Tunable luminescent materials combined with LCs

According to the discussion above in Sections 2 and 3, there are many similarities between the responsive behaviors of  $\text{Ln}^{3+}$ -based luminescent materials and LCs under various external stimuli. Thus, modulation methods for LCs may simultaneously regulate lanthanide luminescence. In addition, LCs can be used as regulatory platforms to affect lanthanide luminescence. For example, LCs can directly regulate the luminescence intensity of  $\text{Ln}^{3+}$  ions by adjusting the polarization characteristics of incident or outgoing light. The transmission and refractive index of the LC phase affect lanthanide luminescence intensity. Thus, by combining these two important functional materials, highly tunable optical properties can be achieved, resulting in fascinating synergistic properties for versatile applications.

Lanthanide luminescence can be introduced into LCs either by the chemical modification of LC molecules or by direct physical mixing.<sup>[113]</sup> In addition, the group orientation arrangement of lanthanide-based materials induced by the LCs phase can maintain their light-polarization characteristics, which provides a good foundation for realizing the synergistic effect of LCs and lanthanide luminescence.<sup>[96,114]</sup>

For instance, Ye et al.<sup>[113b]</sup> proposed a facile strategy for modulating the UCL intensity of UCNPs in LCN composite films and further fabricated UCL patterns. The planar texture of the nematic phase fabricated from a mixture of LC and UCNPs can transform into a homeotropic, planar, and scattering state when treated with strong, no, and weak electric fields, respectively. Under the excitation of a 980 nm laser, strong excitation light scattering occurred in the scattering state with the lowest transparency, which greatly enhanced

the probability of photon absorption by UCNPs, thereby enhancing the UCL intensity. In contrast, the homeotropic state shows the weakest emission intensity due to its high transparency. Benefiting from the different luminescence responses to electric fields, they illustrated potential applications in flexible displays and anti-counterfeiting security films.

High-resolution tomography of flow shear can be realized by monitoring the linearly polarized emission of  $\text{LaPO}_4\text{:Eu}^{3+}$  nanorods in the LCs phase using a confocal microscope.<sup>[29a]</sup> As shown in Figure 8b, the Poiseuille flow of a nanorod dispersion experiences different shear forces along the transverse direction so that the rods will self-assemble into a liquid phase. Thus, using the orientation-dependent linearly polarized emission of  $\text{LaPO}_4\text{:Eu}^{3+}$ , we can sensitively probe the dynamic parameters of fluids.

Recently, in addition to normal CPL, CPL behavior based on the UCL of  $\text{Ln}^{3+}$  (UC-CPL) has been widely studied for various promising applications. Yang et al.<sup>[115]</sup> designed a chiral NLC system with UCNPs and  $\text{CsPbBr}_3$  nanoparticles. Through a rational design,  $\text{CsPbBr}_3$  nanoparticles at the center of the PBG promise high  $g_{\text{lum}}$  values, and UCNPs at the band edge ensure intense emission of  $\text{CsPbBr}_3$  through radiative energy transfer from UCNPs to  $\text{CsPbBr}_3$ . Following a similar mechanism, they utilized the “dual-band-edge enhancement effect” to enhance the UC-CPL performance in UCNP-embedded chiral NLCs, thereby realizing a photonic barcode with multiple encryptions (Figure 8c).<sup>[108]</sup>

#### 5 | ACTIVE METASURFACES

In the last decades, metamaterials have explosively propelled the development of nanoscale optics owing to their excellent characteristics interacting with EM waves.<sup>[6a,30a,31b–d,116]</sup> Metasurfaces, a kind of metamaterials of 2D version, can be formed by artificial building blocks (including dielectric, metallic, and semiconducting materials) of subwavelength-scale, and promise lightweight, compact, and energy-efficient reconfigurable optical systems. Early metasurfaces function for a fixed EM response with a predetermined incident wave as a priori known. When fabricated with rectangular or elliptical meta-atoms, the optical metasurfaces are polarization-dependent and the resonant wavelength is relevant to the dimension of meta-atoms. Tunable metasurfaces with multiple functionalities obtained through the active control of EM waves have attracted considerable attention.

For such tunability, programmable meta-optical elements with arbitrary optical performance can be realized under external stimuli. To achieve this idea, dynamic tuning of the metasurface properties is critical. Adapting to the incident waves with various characteristics and altering the output performances are effective ways to achieve tunable metasurfaces and promote practical applications. Developing reconfigurable optical metasurfaces is a major frontier in



optics and photonics research, development, and commercialization with unparalleled performance and functions that can be dynamically defined on demand. Previous reviews have discussed metasurfaces tuned by various external stimuli; here, we concentrate on the tunable metasurfaces based on four points, including the phase change of metasurfaces, change of surrounding medium refractive index, mechanical tuning of the geometry, and integration metasurfaces with LCs.

## 5.1 | Thermally tunable metasurfaces

Integrating optical phase-change materials (O-PCMs) has been utilized for reconfigurable metasurfaces, endowing photonic elements with versatility and tunability.<sup>[32a,117]</sup> The active metasurfaces consisting of O-PCMs can suffer multilevel and dynamically tunable resonances. Their performance can be reversed by switching the phase state, enabling agile light manipulation.<sup>[118]</sup> For thermal-induced phase change, controlling the temperature and heating/cooling rate shows a great influence on the structure transition of PCMs.<sup>[32c,32d,119]</sup>

Vanadium dioxide ( $\text{VO}_2$ ),  $\text{Ge}_2\text{Sb}_2\text{Te}_5$  (GST),  $\text{Ge}_2\text{Sb}_2\text{Se}_4\text{Te}_1$  (GSST), and other various PCMs are particularly intriguing. By adjusting the temperature, PCMs exhibit distinct properties.  $\text{VO}_2$  is in the insulating state and

with a monoclinic structure at room temperature (300 K).<sup>[119c,119g,119h]</sup> Above 340 K, it transforms into metallic state with a rutile structure. The phase-change critical temperature is low, which is approximately 340 K. Different from  $\text{VO}_2$ , GST, GSST, and other PCMs undergo phase change between amorphous and crystalline states and are influenced by the heating/cooling rate. For GST, the most commonly used material, fully crystalline, partially crystalline, and amorphous states can be obtained in the phase-change process.<sup>[32b,32c,117b-d,119b,119d,120]</sup> Abdollahramezani et al.<sup>[32c]</sup> integrated a robust microheater underneath the GST-based metasurface to control the GST phase states. Amorphous GST was heated above the crystallization temperature ( $\sim 160^\circ\text{C}$ ) for a sufficient time to obtain fully crystallized GST (Figure 9a). By heating above the melting temperature ( $\sim 630^\circ\text{C}$ ) in a short time, the amorphous GST was reversed from the crystalline state after quenching. Similarly, the GSST can also be integrated with a voltage-controlled heater to reversibly switch phases with spatial uniformity.<sup>[32d,32e]</sup> Zhang et al.<sup>[32d]</sup> optimized the electrothermal GSST phase switch and achieved active metasurfaces. The crystallization was realized by applying a long, low-voltage pulse-induced Joule heating via an annealing process, and the amorphization was triggered by a melt-quench process with a short, high-voltage pulse, respectively. Furthermore, reversible PCMs were applied in active metasurfaces to manipulate the amplitude, phase, polarization, and other features of light (Figure 9b).

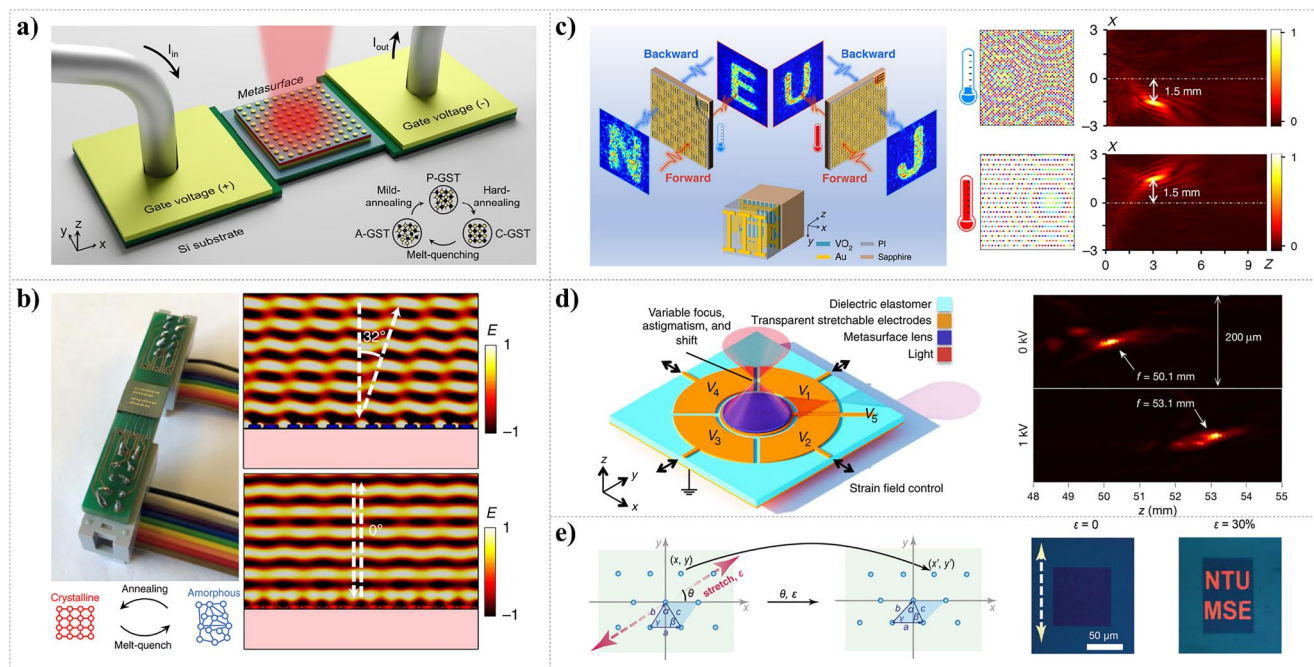


**FIGURE 9** Phase transition and strain-induced active metasurfaces. (a) Integration of a resistive microheater and GST metasurface. Reproduced with permission.<sup>[32c]</sup> Copyright 2022, Springer Nature. (b) Electrothermal phase-change switching configuration of GSST metasurface and its application of the beam deflector. Reproduced with permission.<sup>[32d]</sup> Copyright 2021, Springer Nature. (c) Reconfigurable THz Janus metasurface and differences of spatial phase profiles and simulated electric field distributions of THz wave by phase change. Reproduced with permission.<sup>[119h]</sup> Copyright 2023, Springer Nature. (d) Metalens controlled by an electric-strain field and its tunable performance. Reproduced with permission.<sup>[31a]</sup> Copyright 2018, The American Association for the Advancement of Science. (e) Hexagonal lattice deformation under strain and reflected differential interference contrast under different strains. Scale bar: 50  $\mu\text{m}$ . Reproduced with permission.<sup>[121g]</sup> Copyright 2022, John Wiley and Sons. GST,  $\text{Ge}_2\text{Sb}_2\text{Te}_5$ ; GSST,  $\text{Ge}_2\text{Sb}_2\text{Se}_4\text{Te}_1$ .

Reversible phase change can be achieved rapidly, and the optical properties contrast greatly at different states. Metasurfaces with active tunability have been demonstrated by controlling working temperature. Integrated with VO<sub>2</sub>, a metasurface of broadband polarization states with tunability is demonstrated.<sup>[119g]</sup> By combining the thermal reconfigurability of VO<sub>2</sub> and incident direction dependence of the Janus metasurface, Chen et al.<sup>[119h]</sup> demonstrated a reconfigurable metasurface with four independent EM functionalities (Figure 9c). With optical property contrasting at amorphous and crystalline states (e.g., large refractive index contrast  $\Delta n = 3.56$  at wavelength of 1.55  $\mu\text{m}$ ), GST has been demonstrated to possess tunability and be integrated as meta-devices. The GST was leveraged to dynamically tune the multipolar resonances in different phases. Galarreta et al.<sup>[32b]</sup> designed hybrid metasurfaces, consisting of embedding the GST layer within silicon nanoresonators, and achieved dynamic filtering and modulating light in the NIR region. In addition, the electrothermal phase transition of GST was more convenient. By controlling the applied voltage amplitude and time, arbitrary components of amorphous and crystalline phase states can be fulfilled, which helped to realize an absolute reflectance contrast reaching 80%, a switching speed of a few kHz, and reconfigurable light steering (Figure 9a). Compared to GST, GSST exhibits less absorption loss, while possessing a large refractive index contrast between the two states and broadband transparency. Active metasurfaces optimized by the electrothermal GSST phase switch have been achieved, and the optical phase and wavefront were controlled (Figure 9b). Besides the light steering, other active optical applications have been proposed. Shalaginov et al.<sup>[32e]</sup> demonstrated the varifocal metalens with focal lengths of 1.5 mm at amorphous and 2 mm at the crystalline state, respectively, based on the 16 meta-atom designs for discrete phase values from 0 to  $2\pi$ .

## 5.2 | Strain-modulated metasurfaces

To overcome the static and restricted optical responses of metasurfaces, an active metasurface can be designed with elastomeric substrates for tunable applications.<sup>[121]</sup> Thus, the geometry of metasurfaces is changed by a strain field, which varies the plasmon resonances or Mie resonances as the lattice constant is tuned.<sup>[121e]</sup> The strain field in the tunable substrate can be tuned by the in-plane stretching effect and out-of-plane bending deformation.

For tuning the geometry of metasurfaces, meta-atoms are usually patterned on or encapsulated in the PDMS or other elastomeric substrates. With force to stretch the substrate, the coordinates ( $x$ ,  $y$ ) of the meta-atoms are transformed into ( $x'$ ,  $y'$ ). Correspondingly, the phase profiles  $\phi(x, y)$  of the metasurface are also transformed as  $\phi(x', y')$ . She et al.<sup>[31a]</sup> demonstrated that the strain field of a metalens substrate could be mapped into the output optical wavefront by introducing a transparent polyacrylate elastomer substrate (Figure 9d). Interestingly, deformable metasurfaces can be

described with the crystallographic terminology of 2D Bravais lattices to show the lattice symmetry.<sup>[121g]</sup> The individual particles of the metasurface are embedded in an elastomer and seemed as rigid and nondeformable under the strain. As a result, the coordinates of the particles change with the gradient tensor, and deformation can be applied to obtain arbitrary 2D Bravais lattices (Figure 9e). The decrease in the structure symmetry caused the optical anisotropy upon polarization, which promoted active metasurfaces. In addition to the strain field in-plane, the out-of-plane bending deformation has been applied to active metasurfaces. Karvounis et al.<sup>[122]</sup> demonstrated the mechanical tuning of optical properties with a photonic nanomechanical metasurface composed of MoS<sub>2</sub>/MoO<sub>3-x</sub>/Si<sub>3</sub>N<sub>4</sub> with mechanical bending deformation. The refractive index of MoS<sub>2</sub> changed with the carrier mobility and effective mass of the carriers upon mechanical deformation.

In practical applications, mechanically tunable metasurfaces exhibit versatile functions. She et al. demonstrated that tunable focal length, astigmatism, and image shift corrections could be fulfilled by the strain field of a metalens substrate (Figure 9d). Similarly, Zhang et al.<sup>[121e]</sup> fabricated a metasurface composed of square TiO<sub>2</sub> nanoblocks embedded in PDMS. When the substrate was stretched, the magnetic/electric dipole resonances varied, and further a full visible range response was fulfilled. In addition, active metasurfaces can be fabricated with dynamically actuatable elastomers as substrates. The meta-atoms are deposited on the elastomer substrate, where the incident angle of the beam alters with the substrate bending angle simultaneously. This has been utilized to continuously tune the intensity of the terahertz (THz) wave, as the incident angles change with various banding angles.<sup>[123]</sup> Furthermore, Zhuang et al.<sup>[124]</sup> applied the LCE substrate to tune the incident angle of the metasurface, where the intrinsic bending deformation was caused by the local heating effect of line-focused infrared light, and the THz wavefront steering, frequency modulator, and the tunable beam splitter were modulated.

## 5.3 | Surrounding dielectricity-tuned metasurfaces

Changing the dielectric environment refractive index with gas or liquid immersion is an accessible method for active metasurfaces. Combining metasurfaces with refractive index matching layers would help improve the optical performance according to the intrinsic material loss, broadband spectrum in reflection or transition, and the electric/magnetic dipole mode resonances sensitive to the surrounding medium.<sup>[125]</sup>

Water is usually used to tune the dielectric environment refractive index with metasurfaces.<sup>[125a,125c,126]</sup> Taking the wettability to design multifunctional metasurfaces improves optical performance. Lu et al.<sup>[126a]</sup> demonstrated that when the metasurface was in a superhydrophilic state, the water contact angle (CA) was below 10°, leading to the water droplet fast spread after hydrophilic treatment. Moreover,

hydrophobic treatment would result in metasurface with CA above  $130^\circ$ . Thus, the optical color response of the metasurface differed in the air and water. Considering the water selective wetting property for metals and polymers with hydrophilic/hydrophobic features, Li et al.<sup>[125c]</sup> demonstrated actively switchable beam-steering in two opposite directions. Introducing interfacial phase shifts by metasurfaces can cause the output light in a specific direction. In the dry condition or when immersed in water, the output-reflected beam had a negative angle  $\approx -30^\circ$  and with the opposite orientation of angle  $\approx 30^\circ$ . Moreover, immersion in water or air can result in a high optical contrast of planar optics. Wan et al.<sup>[126c]</sup> endowed a metasurface with different near-field displays and far-field holographic images by switching its dry/wet state of the metasurface. A butterfly was presented with antennas in the air, and a crab was shown in the water for near-field nanoprints. For far-field

holography, an airport and a ship were displayed as determined by the dry and immersed states, respectively.

In addition, other matching layers with various refractive indices show great impacts on active metasurfaces. Dimethyl sulfoxide (DMSO), polymethyl methacrylate, and other fluids can function as refractive index matching layers to improve the optical performance of metasurfaces.<sup>[125a,125b,127]</sup> Yang et al.<sup>[125b]</sup> utilized DMSO ( $n = 1.4$ ) as the refractive matching layer with Si metasurfaces, which distinctly improved the brightness and color purity and reduced the reflected bandwidth and background reflection (Figure 10a). For the structural color display, the gamut increased to approximately 181.8% of sRGB, with DMSO superior to 78% in the air, as the intrinsic loss of Si. Microfluidic or optofluidic metasurfaces with dynamically controlled light fields are interesting for practical applications. For example, Sun et al.<sup>[125a]</sup> applied a metasurface embedded in a polymeric microfluidic

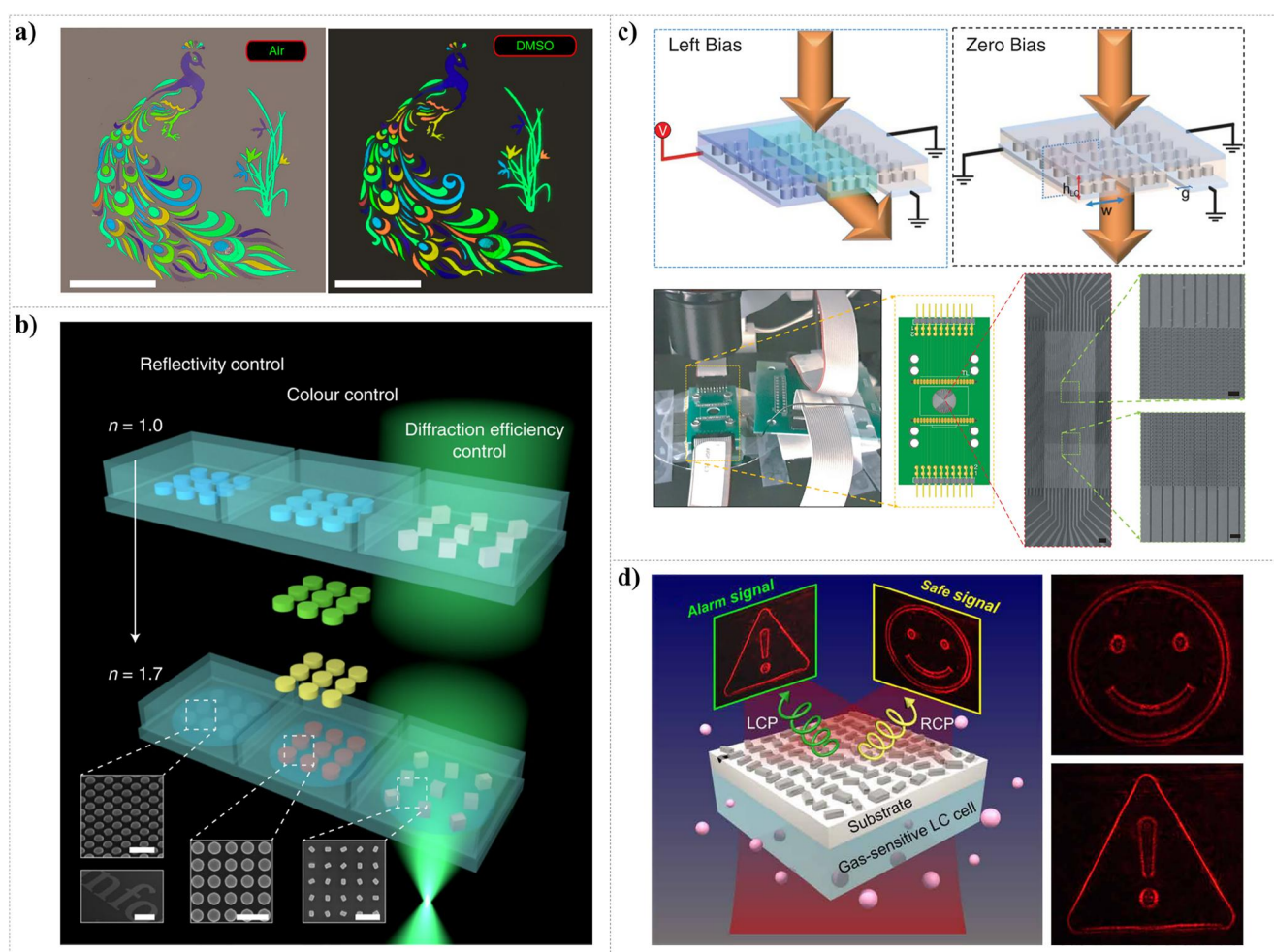


**FIGURE 10** Integration of metasurface and refractive matching layer and LCs. (a) Full-color image printing of metasurface in air and DMSO (function as a refractive matching layer). Scale bar: 100  $\mu\text{m}$ . Reproduced with permission.<sup>[125b]</sup> Copyright 2020, Springer Nature. (b) Si metasurfaces with different environments of refractive index ( $n = 1.0$ – $1.7$ ) around nanoresonators on the same chip. Reproduced with permission.<sup>[127c]</sup> Copyright 2022, Springer Nature. (c) Device mounted for measurements and its operation concept. Reproduced with permission.<sup>[128b]</sup> Copyright 2019, The American Association for the Advancement of Science. (d) The holographic metasurface gas sensor platform exhibiting the initial safety sign and the alarm sign upon the exposure of gases, respectively. Reproduced with permission.<sup>[16b]</sup> Copyright 2021, The American Association for the Advancement of Science. DMSO, dimethyl sulfoxide; LCs, liquid crystals.



channel, and changing the solutions with various refractive indices in the channel resulted in a controllable distinct color. In addition, Li et al.<sup>[127c]</sup> demonstrated metasurface color pixels of tunable intensity and shift spectrum and manipulated the integrated meta-optofluidic platform with a new display function based on the scattering properties of the metasurface sensitive to the dielectric environment. The integrated device comprised metasurfaces inside microfluidic channels and fluids with different refractive indices. In this way, resonant modes experienced less material absorption and resonance shifted to a distinct wavelength with fluid refractive index  $n = 1.7$  compared to  $n = 1$  (Figure 10b).

## 5.4 | Active metasurfaces combined with LCs

Combining LCs with metasurfaces would also give rise to tunability. Upon exposure to external stimuli, LC molecules would reorient, leading to modulate polarization and phase of light, the refractive index of surrounding medium LCs, etc.<sup>[16b,128]</sup>

Optical metasurfaces consisting of anisotropic meta-atoms are polarization-dependent.<sup>[129]</sup> For example, the structural color display can be designed with elliptical meta-atoms in different directions, where the periodic arrangement of the nanopillars with various orientations causes the desired hue and brightness of display colors.<sup>[129c]</sup> Song et al.<sup>[129d]</sup> demonstrated structural color display polarization tunability. Rotating the angle between the incident linearly polarized light and nanoapertures influenced the color brightness. The reflected spectral profiles remained identical at different angles, but the intensity varied. Besides, the geometric phase, or the Pancharatnam–Berry phase, can be obtained by arranging the orientation of antennas of metasurfaces with inversion of the electric field rotation in transmission or reflection.<sup>[30c,30d,129a,129c,130]</sup> Varying the features of the incident wave onto a fixed metasurface can make the output optical properties distinct. Moreover, the integration of metasurfaces and LCs has made great progress in active planar optics.

Tunable phase or polarization can be achieved by external stimuli on LCs, and the practical optical applications are versatile. Shen et al.<sup>[131]</sup> integrated LCs and metalens and accomplished THz metalens with tunable chromatic aberration. In their work, LCs were applied to provide geometric phase modulation, and the metalens was with a resonant phase. By applying voltage, the geometric phase of the LCs disappeared, and the devices became dispersive. When the voltage was off, the device became chromatic by integrating the geometric phase and resonant phase. Dynamic varifocal metalens in the visible range by tuning the polarization of light with various voltages was also demonstrated.<sup>[128c,132]</sup> Besides, the spatial light modulator (SLM) can be designed with precise phase modulation.<sup>[128b,128f]</sup> By tuning the electric field, the alignment directors of LC molecules change, where the effective

refractive index varies, and the precise phase mapping is satisfied as a result. Additionally, by optimizing the design and fabrication process, an SLM of higher resolution was realized to spatially manipulate the phase and polarization of light (Figure 10c).<sup>[128b]</sup> For other applications, active metaholograms and structural colors have also been demonstrated with electric-induced polarization of light.<sup>[51d,128d,132–133]</sup> Interestingly, the optical performance of integrating metasurfaces and LCs can also be tuned by gas, attributing to detecting the biological and harmful chemical materials with metahologram displays. When LC was designed with hybrid alignment and transmitting the right circularly polarized light incidence, the nematic to isotropic phase transition occurred within 40 s when exposed to isopropyl alcohol gas (400 ppm), where the polarization transformed as phase retardation  $\Delta\tau = \pi$ .<sup>[16b]</sup> Thus, the opposite polarization of the incident light made the metaholograms different, which represented a safe signal without volatile gas and an alarm signal with volatile gas (Figure 10d).

Interestingly, the optical properties of metasurfaces infiltrated with LCs show considerable modification according to the sensitivity of metasurface resonances to the refractive index of the surrounding medium.<sup>[128a,134]</sup> With infiltration in NLCs with different refractive indices and birefringence, significant modification of the metalens focus was observed by Lininger et al.<sup>[134b]</sup> In addition, the metasurface system has the potential to enable dynamic reconfigurability, utilizing the tunability of the orientation-dependent refractive index of the infiltrated LC. Furthermore, the high refractive index contrast of LCs obtained by changing the alignment of LC molecules can make the tunable meta-device. Bosch et al.<sup>[128c]</sup> demonstrated varifocal performance by LC-based metalens, where a continuous focal distance shifting from  $f_{\text{off}} = 15$  mm to  $f_{\text{on}} = 12$  mm was achieved. Integrating LCs and metasurfaces makes the optical applications more brilliant and versatile.

## 6 | CONCLUSIONS AND PERSPECTIVES

Light control is of utmost importance in various fields, ranging from scientific research and engineering to everyday technologies and applications. Desired functionalities can be achieved, including focusing light for imaging, steering beams for communication, and selectively filtering light for spectroscopy by controlling parameters, such as intensity, wavelength, polarization, direction, etc. Traditional approaches focus on changing the material properties through the chemical synthesis, while it is important to note that external stimuli and microstructure control also play significant roles in manipulating light. These aspects enable dynamic light manipulation, allowing for the realization of dynamic optical control and contributing to the overall functionality of the optical system. Herein, we focus on optical-inert materials, including LCs, silk proteins, and metasurfaces, as well as the optical-active materials represented by  $\text{Ln}^{3+}$ -based luminescent materials, and provide a

comprehensive presentation of emerging representative physical strategies for controlling their optical properties, such as wavelength/frequency, intensity/amplitude, polarization, phase, angular moment, etc. We discuss the underlying mechanisms of stimuli-responsive features and expect further exploration of manipulating methods. Moreover, composite functional materials with integrated properties are discussed for further advanced and versatile optical applications.

Specifically, conventional LCs exhibit outstanding optical birefringence, flowing features, and stimuli-responsiveness. The optical properties of LCs can be modified by various external fields, including heat, light, electric field, and other stimuli, which show potential for various applications, such as detector, AR/VR, microlens, autonomous actuators, and anti-counterfeiting. In addition, protein-based materials, represented by silk, are another platform for light engineering. Considering that the lattice constant directly determines the optical performance of silk proteins, external stimuli of heat, mechanical strain, light, and chemical treatment is widely utilized to tune the optical performance for smart displays, information processing, and bio-interfaces. Unlike optical-inert materials, luminescent materials are optical-active with self-luminescence. The luminescent parameters, including the emission intensity, emission color, and polarization properties, are highly tunable when external stimuli are applied. Stimuli, including heat, light, electric field, magnetic field, and mechanical stress, are utilized to manipulate the luminescent properties, and the integration of LCs and luminescent materials has been found to be promising and inspire potential applications in displays, information storage, anti-counterfeit, etc. Additionally, metasurfaces have attracted considerable attention owing to their excellent optical performance. The refractive index and lattice constant of meta-atoms and the refractive index matching layer diversification can be regulated, and the electric and magnetic resonance effect of metasurfaces would be tuned by heat, strain field, and varied dielectric environment, which is promising for great performance in metalens, metaholography, structural color, SLM, etc. Combining LCs and metasurfaces can undoubtedly enrich the degree of optical manipulation and trigger fascinating optical properties and advanced applications.

While significant progress has been made and promising potential showcased in the light engineering of various responsive materials, there remains a need for substantial effort to fully leverage composite material systems as combining two or more responsive materials can boost optical performance and release their enormous potential in many application areas. For instance, when integrating LCs with other responsive materials, active planar optics can function with more advanced and versatile performances, promoting tunable photonics research, development, and commercialization. Manipulating the resonances of metasurfaces by integrating them with other materials is also desirable to achieve higher performance.

In addition, the regulation of the optical properties of silk protein is limited to wavelength or structural color.

Manipulating other light parameters, such as amplitude and polarization, remains challenging. Thus, strategies, such as combining photonic crystals with other functional materials, such as LCs, to develop new designs with dynamic polarization sensitivity or amplitude sensitivity, are worth in-depth study. For luminescent materials, utilizing LCs as an optical platform has been demonstrated to be an effective method to manipulate luminescent properties. However, the ambiguous interactions between the LCs and doped luminescent materials limit the exploration of potential applications. Another problem to be solved is how to increase the sensitivity of the stimuli-responsive behavior of luminescent materials. It is worth pointing out that, although composite systems possess better performance, external stimuli may cause complex and various alterations in different responsive materials; thus, systematic and precise work is desired to illustrate the mechanism of optical manipulation under certain stimuli.

## AUTHOR CONTRIBUTIONS

Yan-Qing Lu, Ling-Ling Ma, Yu Wang, and Ling Huang conceived the idea and initiated the project. Ren Zheng, Yang Wei and Zi-Chen Zhang wrote the manuscript. Yan-Qing Lu, Ling-Ling Ma, Yu Wang, Ling Huang, Ren Zheng, Yang Wei, Zi-Chen Zhang, and Ze-Yu Wang revised the manuscript. All the authors participated in the discussion.

## ACKNOWLEDGMENTS

R. Zheng, Y. Wei, and Z. C. Zhang contributed equally to this work. This work was funded by the National Key Research and Development Program of China (Nos. 2022YFA1405000 and 2021YFA1202000), the National Natural Science Foundation of China (Nos. 52003115, 62375119, and 62175102), the Natural Science Foundation of Jiangsu Province, Major Project (No. BK20212004), the Natural Science Foundation of Jiangsu Province (No. BK20200320), the Program for Innovative Talents and Entrepreneurs in Jiangsu (No. JSSCTD202138). L.-L. Ma gratefully acknowledges the support of the Xiaomi Young Scholar Program and Young Elite Scientists Sponsorship Program by CAST (2022QNRC001).

## CONFLICT OF INTEREST STATEMENT

The authors declare no conflict of interest.

## ORCID

Ling-Ling Ma  <https://orcid.org/0000-0002-0001-9524>

## REFERENCES

1. a) M. Kues, C. Reimer, J. M. Lukens, W. J. Munro, A. M. Weiner, D. J. Moss, R. Morandotti, *Nat. Photon.* **2019**, *13*, 170; b) X. Xu, M. Tan, B. Corcoran, J. Wu, A. Boes, T. G. Nguyen, S. T. Chu, B. E. Little, D. G. Hicks, R. Morandotti, A. Mitchell, D. J. Moss, *Nature* **2021**, *589*, 44.
2. a) T. Li, J. Xu, R. Lin, S. Teale, H. Li, Z. Liu, C. Duan, Q. Zhao, K. Xiao, P. Wu, B. Chen, S. Jiang, S. Xiong, H. Luo, S. Wan, L. Li, Q. Bao, Y. Tian, X. Gao, J. Xie, E. H. Sargent, H. Tan, *Nat. Energy* **2023**, *8*, 610; b) R. Lin, Y. Wang, Q. Lu, B. Tang, J. Li, H. Gao, Y. Gao, H. Li, C. Ding, J. Wen, P. Wu, C. Liu, S. Zhao, K. Xiao, Z. Liu, C. Ma, Y. Deng, L. Li, F. Fan, H. Tan, *Nature* **2023**, *620*, 994.

3. a) K. Yin, E. L. Hsiang, J. Zou, Y. Li, Z. Yang, Q. Yang, P. C. Lai, C. L. Lin, S. T. Wu, *Light Sci. Appl.* **2022**, *11*, 161; b) Y. Li, S. Chen, H. Liang, X. Ren, L. Luo, Y. Ling, S. Liu, Y. Su, S.-T. Wu, *Photonix* **2022**, *3*, 29.
4. R. W. Bourdeau, A. Lee-Gosselin, A. Lakshmanan, A. Farhadi, S. R. Kumar, S. P. Nety, M. G. Shapiro, *Nature* **2018**, *553*, 86.
5. a) M. Ku, J. Kim, J. E. Won, W. Kang, Y. G. Park, J. Park, J. H. Lee, J. Cheon, H. H. Lee, J. U. Park, *Sci. Adv.* **2020**, *6*, eabb2891; b) H. Zhu, H. Yang, L. Zhan, Y. Chen, J. Wang, F. Xu, *ACS Sens.* **2022**, *7*, 3014.
6. a) W. T. Chen, A. Y. Zhu, F. Capasso, *Nat. Rev. Mater.* **2020**, *5*, 604; b) W. Lee, Z. Zhou, X. Chen, N. Qin, J. Jiang, K. Liu, M. Liu, T. H. Tao, W. Li, *Nat. Nanotechnol.* **2020**, *15*, 941; c) D. Eliaz, S. Paul, D. Benyamin, A. Cernescu, S. R. Cohen, I. Rosenhek-Goldian, O. Brookstein, M. E. Miali, A. Solomonov, M. Greenblatt, Y. Levy, U. Raviv, A. Barth, U. Shimanovich, *Nat. Commun.* **2022**, *13*, 7856; d) R. S. Zola, H. K. Bisoyi, H. Wang, A. M. Urbas, T. J. Bunning, Q. Li, *Adv. Mater.* **2019**, *31*, 1806172; e) H. K. Bisoyi, T. J. Bunning, Q. Li, *Adv. Mater.* **2018**, *30*, 1706512; f) X. Zhang, Y. Xu, C. Valenzuela, X. Zhang, L. Wang, W. Feng, Q. Li, *Light Sci. Appl.* **2022**, *11*, 223; g) Y. He, S. Lin, J. Guo, Q. Li, *Aggregate* **2021**, *2*, e141.
7. T. H. Ware, M. E. McConney, J. J. Wie, V. P. Tondiglia, T. J. White, *Science* **2015**, *347*, 982.
8. K. Sim, S. Chen, Z. Li, Z. Rao, J. Liu, Y. Lu, S. Jang, F. Ershad, J. Chen, J. Xiao, C. Yu, *Nat. Electron.* **2019**, *2*, 471.
9. a) W. Hu, G. Z. Lum, M. Mastrangeli, M. Sitti, *Nature* **2018**, *554*, 81; b) S. Huang, H. Yu, Q. Li, *Adv. Sci.* **2021**, *8*, 2002132.
10. Z. Liu, H. K. Bisoyi, Y. Huang, M. Wang, H. Yang, Q. Li, *Angew. Chem., Int. Ed.* **2022**, *61*, e202115755.
11. J. Yang, X. Zhang, X. Zhang, L. Wang, W. Feng, Q. Li, *Adv. Mater.* **2021**, *33*, 2004754.
12. a) W. Li, Y. Wang, M. Li, L. P. Garbarini, F. G. Omenetto, *Adv. Mater.* **2019**, *31*, 1901036; b) S. Huang, Y. Huang, Q. Li, *Small Struct.* **2021**, *2*, 2100038.
13. a) *Fundamentals of Liquid Crystal Devices* (Eds: S. T. Wu, D. K. Yang), John Wiley & Sons, West Sussex, England, UK **2014**; b) *Liquid Crystals beyond Displays: Chemistry, Physics, and Applications* (Ed: Q. Li), John Wiley & Sons, Hoboken, NJ **2012**; c) *Nanoscience with Liquid Crystals: From Self-Organized Nanostructures to Applications* (Ed: Q. Li), Springer, Heidelberg **2014**.
14. a) H. K. Bisoyi, Q. Li, *Chem. Rev.* **2022**, *122*, 4887; b) L.-L. Ma, C. Liu, S.-B. Wu, P. Chen, Q.-M. Chen, J.-X. Qian, S.-J. Ge, Y.-H. Wu, W. Hu, Y.-Q. Lu, *Sci. Adv.* **2021**, *7*, eabh3505.
15. a) H. K. Bisoyi, Q. Li, *Acc. Chem. Res.* **2014**, *47*, 3184; b) P. Chen, B. Y. Wei, W. Hu, Y. Q. Lu, *Adv. Mater.* **2020**, *32*, 1903665; c) Z. G. Zheng, Y. Q. Lu, Q. Li, *Adv. Mater.* **2020**, *32*, 1905318; d) L.-L. Ma, W. Duan, M.-J. Tang, L.-J. Chen, X. Liang, Y.-Q. Lu, W. Hu, *Polymers* **2017**, *9*, 295; e) L.-L. Ma, W. Hu, Z.-G. Zheng, S.-B. Wu, P. Chen, Q. Li, Y.-Q. Lu, *Adv. Opt. Mater.* **2019**, *7*, 1900393; f) Y. Wang, C. L. Yuan, W. Huang, P. Z. Sun, B. Liu, H. L. Hu, Z. Zheng, Y. Q. Lu, Q. Li, *Adv. Mater.* **2023**, *35*, 2211521.
16. a) P. Chen, L.-L. Ma, W. Hu, Z.-X. Shen, H. K. Bisoyi, S. B. Wu, S.-J. Ge, Q. Li, Y.-Q. Lu, *Nat. Commun.* **2019**, *10*, 2518; b) I. Kim, W. S. Kim, K. Kim, M. A. Ansari, M. Q. Mehmood, T. Badloe, Y. Kim, J. Gwak, H. Lee, Y. K. Kim, J. Rho, *Sci. Adv.* **2021**, *7*, eabe9943; c) Y. Liu, W. Chen, J. Tang, X. Xu, P. Chen, C. Q. Ma, W. Zhang, B. Y. Wei, Y. Ming, G. X. Cui, Y. Zhang, W. Hu, Y. Q. Lu, *Adv. Opt. Mater.* **2020**, *9*, 2001776; d) J. A. Lv, Y. Liu, J. Wei, E. Chen, L. Qin, Y. Yu, *Nature* **2016**, *537*, 179.
17. a) L.-Y. Sun, X.-Y. Wang, J.-H. Chen, C.-Y. Li, L.-L. Ma, Y.-Q. Lu, B.-X. Li, *J. Mol. Liq.* **2022**, *363*, 119843; b) Z. Song, Z. Li, X. Shang, C. Li, L. Ma, Y. Lu, B. Li, *Chin. Opt. Lett.* **2023**, *21*, 010501; c) R. Zheng, L. Ma, W. Feng, J. Pan, Z. Wang, Z. Chen, Y. Zhang, C. Li, P. Chen, H. K. Bisoyi, B. Li, Q. Li, Y. Lu, *Adv. Funct. Mater.* **2023**, *33*, 2301142; d) R. Chen, Y. H. Lee, T. Zhan, K. Yin, Z. An, S. T. Wu, *Adv. Opt. Mater.* **2019**, *7*, 1900101; e) B.-X. Li, R.-L. Xiao, S. Paladugu, S. V. Shivanovskii, O. D. Lavrentovich, *Nat. Commun.* **2019**, *10*, 3749; f) D. Franklin, R. Frank, S. T. Wu, D. Chanda, *Nat. Commun.* **2017**, *8*, 15209; g) L.-L. Ma, M.-J. Tang, W. Hu, Z.-Q. Cui, S.-J. Ge, P. Chen, L.-J. Chen, H. Qian, L.-F. Chi, Y.-Q. Lu, *Adv. Mater.* **2017**, *29*, 1606671.
18. a) F. Vollrath, D. P. Knight, *Nature* **2001**, *410*, 541; b) H. J. Jin, D. L. Kaplan, *Nature* **2003**, *424*, 1057;
19. a) Z. Shao, F. Vollrath, *Nature* **2002**, *418*, 741; b) J. L. Yarger, B. R. Cherry, A. van der Vaart, *Nat. Rev. Mater.* **2018**, *3*, 18008.
20. a) D. F. Williams, *Biomaterials* **2008**, *29*, 2941; b) D. F. Williams, *Biomaterials* **2014**, *35*, 10009.
21. a) M. Li, M. Ogiso, N. Minoura, *Biomaterials* **2003**, *24*, 357; b) H. Tao, J. M. Kainerstorfer, S. M. Siebert, E. M. Pritchard, A. Sassaroli, B. J. Panilaitis, M. A. Brenckle, J. J. Amsden, J. Levitt, S. Fantini, D. L. Kaplan, F. G. Omenetto, *Proc. Natl. Acad. Sci. U. S. A.* **2012**, *109*, 19584.
22. a) L. Xu, X. Jiang, G. Zhao, D. Ma, H. Tao, Z. Liu, F. G. Omenetto, L. Yang, *Opt. Express* **2016**, *24*, 20825; b) K. Min, S. Kim, S. Kim, *Proc. Natl. Acad. Sci. U. S. A.* **2017**, *114*, 6185; c) H. S. Kim, S. H. Cha, B. Roy, S. Kim, Y. H. Ahn, *Opt. Express* **2018**, *26*, 33575.
23. Z. Zhou, Z. Shi, X. Cai, S. Zhang, S. G. Corder, X. Li, Y. Zhang, G. Zhang, L. Chen, M. Liu, D. L. Kaplan, F. G. Omenetto, Y. Mao, Z. Tao, T. H. Tao, *Adv. Mater.* **2017**, *29*, 1605471.
24. H. Tao, D. L. Kaplan, F. G. Omenetto, *Adv. Mater.* **2012**, *24*, 2824.
25. C. Guo, C. Li, X. Mu, D. L. Kaplan, *Appl. Phys. Rev.* **2020**, *7*, 011313.
26. a) F. Auzel, *Chem. Rev.* **2004**, *104*, 139; b) K. Zhang, X. Xie, H. Li, J. Gao, L. Nie, Y. Pan, J. Xie, D. Tian, W. Liu, Q. Fan, H. Su, L. Huang, W. Huang, *Adv. Mater.* **2017**, *29*, 1701804; c) D. Tian, F. Qi, H. Ma, X. Wang, Y. Pan, R. Chen, Z. Shen, Z. Liu, L. Huang, W. Huang, *Nat. Commun.* **2018**, *9*, 2688; d) L. Wang, S. Guo, D. Liu, J. He, J. Zhou, K. Zhang, Y. Wei, Y. Pan, C. Gao, Z. Yuan, D. Lei, X. Xie, L. Huang, *Adv. Funct. Mater.* **2019**, *29*, 1901242; e) X. Cheng, J. Zhou, J. Yue, Y. Wei, C. Gao, X. Xie, L. Huang, *Chem. Rev.* **2022**, *122*, 15998.
27. a) X. Liu, Y. Wang, X. Li, Z. Yi, R. Deng, L. Liang, X. Xie, D. T. B. Loong, S. Song, D. Fan, A. H. All, H. Zhang, L. Huang, X. Liu, *Nat. Commun.* **2017**, *8*, 899; b) H. Ge, D. Wang, Y. Pan, Y. Guo, H. Li, F. Zhang, X. Zhu, Y. Li, C. Zhang, L. Huang, *Angew. Chem., Int. Ed.* **2020**, *59*, 8133; c) J. Zhou, Y. Wei, Y. Pan, Y. Wang, Z. Yuan, F. Zhang, H. Song, J. Yue, H. Su, X. Xie, L. Huang, *Nat. Commun.* **2021**, *12*, 2948; d) Y. Hao, L. Wang, L. F. Huang, *Nat. Commun.* **2023**, *14*, 3256; e) L. Yi, B. Hou, H. Zhao, X. Liu, *Nature* **2023**, *618*, 281.
28. a) Z. Yuan, L. Zhang, S. Li, W. Zhang, M. Lu, Y. Pan, X. Xie, L. Huang, W. Huang, *J. Am. Chem. Soc.* **2018**, *140*, 15507; b) C. Gao, Y. Han, K. Zhang, T. Wei, Z. Jiang, Y. Wei, L. Yin, F. Piccinelli, C. Yao, X. Xie, M. Bettinelli, L. Huang, *Adv. Sci.* **2020**, *7*, 2002444; c) H. Li, X. Liu, Q. Ying, C. Wang, W. Jia, X. Xing, L. Yin, Z. Lu, K. Zhang, Y. Pan, Z. Shi, L. Huang, D. Jia, *Angew. Chem., Int. Ed.* **2020**, *59*, 17207; d) W. Kang, X. Gao, H. Li, Y. Wei, C. Wang, Z. Tian, *Adv. Funct. Mater.* **2023**, *33*, 2300388; e) H. Amouri, *Chem. Rev.* **2023**, *123*, 230.
29. a) J. Kim, S. Michelin, M. Hilbers, L. Martinelli, E. Chaudan, G. Amselem, E. Fradet, J. P. Boilot, A. M. Brouwer, C. N. Baroud, J. Peretti, T. Gacoin, *Nat. Nanotechnol.* **2017**, *12*, 914; b) Y. Yang, J. Huang, W. Wei, Q. Zeng, X. Li, D. Xing, B. Zhou, T. Zhang, *Nat. Commun.* **2022**, *13*, 3149.
30. a) A. S. Solntsev, G. S. Agarwal, Y. S. Kivshar, *Nat. Photon.* **2021**, *15*, 327; b) X. Zhang, Y. Liu, J. Han, Y. Kivshar, Q. Song, *Science* **2022**, *377*, 1215; c) Y. Intaravanne, R. Wang, H. Ahmed, Y. Ming, Y. Zheng, Z. K. Zhou, Z. Li, S. Chen, S. Zhang, X. Chen, *Light Sci. Appl.* **2022**, *11*, 302; d) X. Zhang, L. Huang, R. Zhao, H. Zhou, X. Li, G. Geng, J. Li, X. Li, Y. Wang, S. Zhang, *Sci. Adv.* **2022**, *8*, eabp8073.
31. a) A. She, S. Zhang, S. Shian, D. R. Clarke, F. Capasso, *Sci. Adv.* **2018**, *4*, eaap9957; b) T. Badloe, J. Lee, J. Seong, J. Rho, *Adv. Photonics Res.* **2021**, *2*, 2000205; c) J. Kim, J. Seong, Y. Yang, S.-W. Moon, T. Badloe, J. Rho, *Adv. Photonics* **2022**, *4*, 024001; d) D. N. Neshev, A. E. Miroshnichenko, *Nat. Photon.* **2022**, *17*, 26.

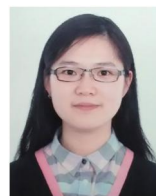


32. a) M. Wuttig, H. Bhaskaran, T. Taubner, *Nat. Photon.* **2017**, *11*, 465; b) C. Ruiz de Galarreta, I. Sinev, A. M. Alexeev, P. Trofimov, K. Ladutenko, S. Garcia-Cuevas Carrillo, E. Gemo, A. Baldycheva, J. Bertolotti, C. David Wright, *Optica* **2020**, *7*, 476; c) S. Abdollahramezani, O. Hemmaty, M. Taghinejad, H. Taghinejad, A. Krasnok, A. A. Eftekhar, C. Teichrib, S. Deshmukh, M. A. El-Sayed, E. Pop, M. Wuttig, A. Alu, W. Cai, A. Adibi, *Nat. Commun.* **2022**, *13*, 1696; d) Y. Zhang, C. Fowler, J. Liang, B. Azhar, M. Y. Shalaginov, S. Deckoff-Jones, S. An, J. B. Chou, C. M. Roberts, V. Liberman, M. Kang, C. Rios, K. A. Richardson, C. Rivero-Baleine, T. Gu, H. Zhang, J. Hu, *Nat. Nanotechnol.* **2021**, *16*, 661; e) M. Y. Shalaginov, S. An, Y. Zhang, F. Yang, P. Su, V. Liberman, J. B. Chou, C. M. Roberts, M. Kang, C. Rios, Q. Du, C. Fowler, A. Agarwal, K. A. Richardson, C. Rivero-Baleine, H. Zhang, J. Hu, T. Gu, *Nat. Commun.* **2021**, *12*, 1225.
33. a) L.-L. Ma, C.-Y. Li, J.-T. Pan, Y.-E. Ji, C. Jiang, R. Zheng, Z.-Y. Wang, Y. Wang, B.-X. Li, Y.-Q. Lu, *Light Sci. Appl.* **2022**, *11*, 270; b) H. K. Bisoyi, Q. Li, *Chem. Rev.* **2016**, *116*, 15089; c) Z. Zhou, S. Zhang, Y. Cao, B. Marelli, X. Xia, T. H. Tao, *Adv. Mater.* **2018**, *30*, 1706983; d) H. A. Nguyen, G. Dixon, F. Y. Dou, S. Gallagher, S. Gibbs, D. M. Ladd, E. Marino, J. C. Ondry, J. P. Shanahan, E. S. Vasileiadou, S. Barlow, D. R. Gamelin, D. S. Ginger, D. M. Jonas, M. G. Kanatzidis, S. R. Marder, D. Morton, C. B. Murray, J. S. Owen, D. V. Talapin, M. F. Toney, B. M. Cossairt, *Chem. Rev.* **2023**, *123*, 7890; e) T. Gu, H. J. Kim, C. Rivero-Baleine, J. Hu, *Nat. Photon.* **2022**, *17*, 48.
34. a) B. Liu, C. L. Yuan, H. L. Hu, H. Wang, Y. W. Zhu, P. Z. Sun, Z. Y. Li, Z. G. Zheng, Q. Li, *Nat. Commun.* **2022**, *13*, 2712; b) L. Ma, C. Li, L. Sun, Z. Song, Y. Lu, B. Li, *Photon. Res.* **2022**, *10*, 786; c) S. U. Kim, Y. J. Lee, J. Liu, D. S. Kim, H. Wang, S. Yang, *Nat. Mater.* **2022**, *21*, 41; d) O. M. Wani, R. Verpaalen, H. Zeng, A. Priimagi, A. Schenning, *Adv. Mater.* **2019**, *31*, 1805985; e) R. Lan, Q. Wang, C. Shen, R. Huang, J. Bao, Z. Zhang, L. Zhang, H. Yang, *Adv. Funct. Mater.* **2021**, *31*, 2106419; f) H. Wang, H. K. Bisoyi, M. E. McConney, A. M. Urbas, T. J. Bunning, Q. Li, *Adv. Mater.* **2019**, *31*, 1902958; g) J. Xiang, S. V. Shiyantovskii, C. Imrie, O. D. Lavrentovich, *Phys. Rev. Lett.* **2014**, *112*, 217801.
35. a) P. Chen, W. Ji, B.-Y. Wei, W. Hu, V. Chigrinov, Y.-Q. Lu, *Appl. Phys. Lett.* **2015**, *107*, 241102; b) B.-Y. Wei, P. Chen, S.-J. Ge, L.-C. Zhang, W. Hu, Y.-Q. Lu, *Photon. Res.* **2016**, *4*, 70.
36. Z. Zheng, H. Hu, Z. Zhang, B. Liu, M. Li, D.-H. Qu, H. Tian, W.-H. Zhu, B. L. Feringa, *Nat. Photon.* **2022**, *16*, 226.
37. a) W. Hu, L. Wang, M. Wang, T. Zhong, Q. Wang, L. Zhang, F. Chen, K. Li, Z. Miao, D. Yang, H. Yang, *Nat. Commun.* **2021**, *12*, 1440; b) Y. Yang, L. Wang, H. Yang, Q. Li, *Small Sci.* **2021**, *1*, 2100007.
38. S. B. Wu, J. B. Wu, H. M. Cao, Y. Q. Lu, W. Hu, *Phys. Rev. Lett.* **2023**, *130*, 078101.
39. a) S. Lin, Y. Tang, W. Kang, H. K. Bisoyi, J. Guo, Q. Li, *Nat. Commun.* **2023**, *14*, 3005; b) Y.-H. Zhang, P. Chen, C.-T. Xu, L. Zhu, X.-Y. Wang, S.-J. Ge, W. Hu, Y.-Q. Lu, *ACS Photonics* **2022**, *9*, 1050; c) D. Franklin, Y. Chen, A. Vazquez-Guardado, S. Modak, J. Boroumand, D. Xu, S. T. Wu, D. Chanda, *Nat. Commun.* **2015**, *6*, 7337; d) H. Wang, H. K. Bisoyi, L. Wang, A. M. Urbas, T. J. Bunning, Q. Li, *Angew. Chem., Int. Ed.* **2018**, *57*, 1627.
40. a) B. Basnet, M. Rajabi, H. Wang, P. Kumari, K. Thapa, S. Paul, M. O. Lavrentovich, O. D. Lavrentovich, *Nat. Commun.* **2022**, *13*, 3932; b) X. Zhan, Z. Zhou, W. Zhou, Y. Yan, J. Yao, Y. S. Zhao, *Adv. Opt. Mater.* **2022**, *11*, 2200872; c) M.-C. Yeh, S.-H. Yang, W. Lee, *J. Mol. Liq.* **2019**, *296*, 112082; d) J. Li, H. Nishikawa, J. Kougo, J. Zhou, S. Dai, W. Tang, X. Zhao, Y. Hisai, M. Huang, S. Aya, *Sci. Adv.* **2021**, *7*, eabf5047; e) X. Chen, E. Korblova, D. Dong, X. Wei, R. Shao, L. Radzihovsky, M. A. Glaser, J. E. MacLennan, D. Bedrov, D. M. Walba, N. A. Clark, *Proc. Natl. Acad. Sci. U. S. A.* **2020**, *117*, 14021; f) S. J. Liu, L. Zhu, Y. H. Zhang, W. Chen, D. Zhu, P. Chen, Y. Q. Lu, *Adv. Mater.* **2023**, *35*, 2301714.
41. L. L. Ma, S. B. Wu, W. Hu, C. Liu, P. Chen, H. Qian, Y. Wang, L. Chi, Y. Q. Lu, *ACS Nano* **2019**, *13*, 13709.
42. a) X. Chen, E. Korblova, M. A. Glaser, J. E. MacLennan, D. M. Walba, N. A. Clark, *Proc. Natl. Acad. Sci. U. S. A.* **2021**, *118*, e2104092118; b) X. Zhao, J. Zhou, J. Li, J. Kougo, Z. Wan, M. Huang, S. Aya, *Proc. Natl. Acad. Sci. U. S. A.* **2021**, *118*, e2111101118.
43. X. Zhao, H. Long, H. Xu, J. Kougo, R. Xia, J. Li, M. Huang, S. Aya, *Proc. Natl. Acad. Sci. U. S. A.* **2022**, *119*, e2205636119.
44. a) Z. Hu, Y. Li, J. A. Lv, *Nat. Commun.* **2021**, *12*, 3211; b) A. H. Gelebart, D. Jan Mulder, M. Varga, A. Konya, G. Vantomme, E. W. Meijer, R. L. B. Selinger, D. J. Broer, *Nature* **2017**, *546*, 632; c) Y. Li, Y. Liu, D. Luo, *Adv. Opt. Mater.* **2020**, *9*, 2001861; d) Z. G. Zheng, Y. Li, H. K. Bisoyi, L. Wang, T. J. Bunning, Q. Li, *Nature* **2016**, *531*, 352; e) Q. Li, A. P. H. J. Schenning, T. J. Bunning, *Adv. Opt. Mater.* **2019**, *7*, 1901160.
45. a) K. Zhou, H. K. Bisoyi, J. Q. Jin, C. L. Yuan, Z. Liu, D. Shen, Y. Q. Lu, Z. G. Zheng, W. Zhang, Q. Li, *Adv. Mater.* **2018**, *30*, e1800237; b) J. R. Talukder, H. Y. Lin, S. T. Wu, *Opt. Express* **2019**, *27*, 18169; c) L. Wang, A. M. Urbas, Q. Li, *Adv. Mater.* **2020**, *32*, 1801335; d) Q. Wang, L. Yu, J. Sun, Y. Guan, Z. Zhou, Y. Shin, H. Yang, J. West, D. K. Yang, *Adv. Opt. Mater.* **2020**, *8*, 2001207; e) X. Zhang, B. Koz, H. K. Bisoyi, H. Wang, K. G. Gutierrez-Cuevas, M. E. McConney, T. J. Bunning, Q. Li, *ACS Appl. Mater. Interfaces* **2020**, *12*, 55215; f) Y. He, S. Zhang, H. K. Bisoyi, J. Qiao, H. Chen, J. Gao, J. Guo, Q. Li, *Angew. Chem., Int. Ed.* **2021**, *60*, 27158; g) J. Pan, J. Qian, L. Ma, Z. Wang, R. Zheng, N. Wang, B. Li, Y. Lu, *Chin. Opt. Lett.* **2023**, *21*, 041603.
46. H. Wang, H. K. Bisoyi, B. X. Li, M. E. McConney, T. J. Bunning, Q. Li, *Angew. Chem., Int. Ed.* **2020**, *59*, 2684.
47. H. Wang, Y. Tang, H. Krishna Bisoyi, Q. Li, *Angew. Chem., Int. Ed.* **2023**, *62*, e202216600.
48. A. S. Kuenstler, H. Kim, R. C. Hayward, *Adv. Mater.* **2019**, *31*, 1901216.
49. L. Qin, W. Gu, J. Wei, Y. Yu, *Adv. Mater.* **2018**, *30*, 1704941.
50. R. Williams, *J. Chem. Phys.* **1963**, *39*, 384.
51. a) L.-L. Ma, S.-S. Li, W.-S. Li, W. Ji, B. Luo, Z.-G. Zheng, Z.-P. Cai, V. Chigrinov, Y.-Q. Lu, W. Hu, L.-J. Chen, *Adv. Opt. Mater.* **2015**, *3*, 1691; b) Y.-C. Hsiao, Z.-H. Yang, D. Shen, W. Lee, *Adv. Opt. Mater.* **2018**, *6*, 1701128; c) K. Chen, C. Xu, Z. Zhou, Z. Li, P. Chen, G. Zheng, W. Hu, Y. Lu, *Laser Photonics Rev.* **2022**, *16*, 2100591; d) J. Wang, W. Cai, H. He, M. Cen, J. Liu, D. Kong, D. Luo, Y. Q. Lu, Y. J. Liu, *Nanoscale* **2022**, *14*, 17921; e) J. B. Wu, S. B. Wu, H. M. Cao, Q. M. Chen, Y. Q. Lu, W. Hu, *Adv. Opt. Mater.* **2022**, *10*, 2201015.
52. C. T. Xu, B. H. Liu, C. Peng, Q. M. Chen, P. Chen, P. Z. Sun, Z. G. Zheng, Y. Q. Lu, W. Hu, *Adv. Opt. Mater.* **2022**, *10*, 2201088.
53. C. T. Xu, D. W. Zhang, R. Yuan, Q. M. Chen, X. Liang, W. Hu, *Laser Photonics Rev.* **2023**, *17*, 2201013.
54. D. Franklin, Z. He, P. Mastranzo Ortega, A. Safaei, P. Cencillo-Abad, S. T. Wu, D. Chanda, *Proc. Natl. Acad. Sci. U. S. A.* **2020**, *117*, 13350.
55. a) P. Zhang, X. Shi, A. P. H. J. Schenning, G. Zhou, L. T. Haan, *Adv. Mater. Interfaces* **2019**, *7*, 1901878; b) Z. X. Shen, M. J. Tang, P. Chen, S. H. Zhou, S. J. Ge, W. Duan, T. Wei, X. Liang, W. Hu, Y. Q. Lu, *Adv. Opt. Mater.* **2020**, *8*, 1902124; c) T. H. Ware, J. S. Biggins, A. F. Shick, M. Warner, T. J. White, *Nat. Commun.* **2016**, *7*, 10781.
56. a) J. A. H. P. Sol, L. G. Smits, A. P. H. J. Schenning, M. G. Debije, *Adv. Funct. Mater.* **2022**, *32*, 2201766; b) S. Hussain, S. Y. Park, *ACS Appl. Mater. Interfaces* **2021**, *13*, 59275; c) C. Sun, S. Zhang, Y. Ren, J. Zhang, J. Shen, S. Qin, W. Hu, S. Zhu, H. Yang, D. Yang, *Adv. Sci.* **2022**, *9*, 2205325; d) S. Nam, D. Wang, C. Kwon, S. H. Han, S. S. Choi, *Adv. Mater.* **2023**, *35*, 2302456.
57. a) S. Tadeipalli, J. M. Slocik, M. K. Gupta, R. R. Naik, S. Singamaneni, *Chem. Rev.* **2017**, *117*, 12705; b) G. Guidetti, F. G. Omenetto, *MRS Commun.* **2020**, *10*, 201.
58. Y. Wang, M. Li, Y. Wang, *Chin. Opt. Lett.* **2020**, *18*, 080004.
59. T. Asakura, Y. Sato, A. Aoki, *Macromolecules* **2015**, *48*, 5761.
60. E. Colusso, G. Perotto, Y. Wang, M. Sturaro, F. Omenetto, A. Martucci, *J. Mater. Chem. C* **2017**, *5*, 3924.

61. X. Cai, Z. Zhou, T. H. Tao, *Adv. Sci.* **2019**, *6*, 1801746.
62. G. Guidetti, Y. Wang, F. G. Omenetto, *Nanophotonics* **2020**, *10*, 137.
63. a) A. P. C. Almeida, J. P. Canejo, S. N. Fernandes, C. Echeverria, P. L. Almeida, M. H. Godinho, *Adv. Mater.* **2018**, *30*, 1703655; b) C. Xu, C. Huang, H. Huang, *Appl. Mater. Today* **2021**, *22*, 100912; c) Z. Peng, Q. Lin, Y. A. Tai, Y. Wang, *J. Agric. Food Chem.* **2020**, *68*, 12940.
64. a) J. Shao, J. Zheng, J. Liu, C. M. Carr, *J. Appl. Polym. Sci.* **2005**, *96*, 1999; b) X. Hu, K. Shmelev, L. Sun, E. S. Gil, S. H. Park, P. Cebe, D. L. Kaplan, *Biomacromolecules* **2011**, *12*, 1686.
65. c) Y. Wang, D. Aurelio, W. Li, P. Tseng, Z. Zheng, M. Li, D. L. Kaplan, M. Liscidini, F. G. Omenetto, *Adv. Mater.* **2017**, *29*, 1702769.
66. Q. Li, N. Qi, Y. Peng, Y. Zhang, L. Shi, X. Zhang, Y. Lai, K. Wei, I. S. Kim, K.-Q. Zhang, *RSC Adv.* **2017**, *7*, 17889.
67. S. T. Parker, P. Domachuk, J. Amsden, J. Bressner, J. A. Lewis, D. L. Kaplan, F. G. Omenetto, *Adv. Mater.* **2009**, *21*, 2411.
68. a) H. Kwon, S. Kim, *ACS Photonics* **2015**, *2*, 1675; b) S. Arif, M. Umar, S. Kim, *ACS Omega* **2019**, *4*, 9010.
69. M. Lee, H. Jeon, S. Kim, *Nano Lett.* **2015**, *15*, 3358.
70. L. Sun, Z. Zhou, J. Zhong, Z. Shi, Y. Mao, H. Li, J. Cao, T. H. Tao, *Small* **2020**, *16*, 2000294.
71. C. Cheng, Y. Qiu, S. Tang, B. Lin, M. Guo, B. Gao, B. He, *Adv. Funct. Mater.* **2021**, *32*, 2107707.
72. Y. Wang, J. Ren, C. Ye, Y. Pei, S. Ling, *Nano-Micro Lett.* **2021**, *13*, 72.
73. W. Zheng, X. Cai, D. Yan, G. Murtaza, Z. Meng, L. Qiu, *Gels* **2022**, *8*, 339.
74. Y. Wang, B. J. Kim, B. Peng, W. Li, Y. Wang, M. Li, F. G. Omenetto, *Proc. Natl. Acad. Sci. U. S. A.* **2019**, *116*, 21361.
75. Y. Wang, B. J. Kim, G. Guidetti, F. G. Omenetto, *Small* **2022**, *18*, 2201036.
76. a) K. Yu, T. Fan, S. Lou, D. Zhang, *Prog. Mater. Sci.* **2013**, *58*, 825. b) H. Zhou, J. Xu, X. Liu, H. Zhang, D. Wang, Z. Chen, D. Zhang, T. Fan, *Adv. Funct. Mater.* **2017**, *28*, 1705309.
77. Y. Wang, M. Li, J. K. Chang, D. Aurelio, W. Li, B. J. Kim, J. H. Kim, M. Liscidini, J. A. Rogers, F. G. Omenetto, *Nat. Commun.* **2021**, *12*, 1651.
78. a) M. Cronin-Golomb, A. R. Murphy, J. P. Mondia, D. L. Kaplan, F. G. Omenetto, *J. Polym. Sci., Part B: Polym. Phys.* **2012**, *50*, 257; b) M. J. Landry, M. B. Applegate, O. S. Bushuyev, F. G. Omenetto, D. L. Kaplan, M. Cronin-Golomb, C. J. Barrett, *Soft Matter* **2017**, *13*, 2903; c) G. Palermo, L. Barberi, G. Perotto, R. Caputo, L. De Sio, C. Umeton, F. G. Omenetto, *ACS Appl. Mater. Interfaces* **2017**, *9*, 30951.
79. H. Zhang, L. Cao, J. Li, Y. Liu, Z. Lv, J. Ren, Z. Shao, S. Ling, *Chem. Mater.* **2023**, *35*, 1752.
80. B. Zheng, J. Fan, B. Chen, X. Qin, J. Wang, F. Wang, R. Deng, X. Liu, *Chem. Rev.* **2022**, *122*, 5519.
81. Y. Wei, Y. Pan, E. Zhou, Z. Yuan, H. Song, Y. Wang, J. Zhou, J. Rui, M. Xu, L. Ning, Z. Liu, H. Wang, X. Xie, X. Tang, H. Su, X. Xing, L. Huang, *Angew. Chem., Int. Ed.* **2023**, *62*, e202303482.
82. X. Zhou, L. Ning, J. Qiao, Y. Zhao, P. Xiong, Z. Xia, *Nat. Commun.* **2022**, *13*, 7589.
83. D. Denkova, M. Ploschner, M. Das, L. M. Parker, X. Zheng, Y. Lu, A. Orth, N. H. Packer, J. A. Piper, *Nat. Commun.* **2019**, *10*, 3695.
84. D. Yang, Z. Peng, Q. Zhan, X. Huang, X. Peng, X. Guo, G. Dong, J. Qiu, *Small* **2019**, *15*, 1904298.
85. a) C. D. S. Brites, S. Balabhadra, L. D. Carlos, *Adv. Opt. Mater.* **2018**, *7*, 1801239; b) X. Wu, S. Zhan, J. Han, Y. Liu, *Nano Lett.* **2021**, *21*, 272.
86. P. Dang, W. Wang, H. Lian, G. Li, J. Lin, *Adv. Opt. Mater.* **2022**, *10*, 2102287.
87. L. Chen, X. Chen, R. Ma, K. Lin, Q. Li, J. P. Lang, C. Liu, K. Kato, L. Huang, X. Xing, *J. Am. Chem. Soc.* **2022**, *144*, 13688.
88. a) Y. Hu, Q. Shao, P. Zhang, Y. Dong, F. Fang, J. Jiang, *J. Phys. Chem. C* **2018**, *122*, 26142; b) J. Zhou, S. Wen, J. Liao, C. Clarke, S. A. Tawfik, W. Ren, C. Mi, F. Wang, D. Jin, *Nat. Photon.* **2018**, *12*, 154.
89. Y. H. Kim, P. Arunkumar, B. Y. Kim, S. Unithrattil, E. Kim, S. H. Moon, J. Y. Hyun, K. H. Kim, D. Lee, J. S. Lee, W. B. Im, *Nat. Mater.* **2017**, *16*, 543.
90. X. Cheng, H. Ge, Y. Wei, K. Zhang, W. Su, J. Zhou, L. Yin, Q. Zhan, S. Jing, L. Huang, *ACS Nano* **2018**, *12*, 10992.
91. Y. Pan, X. Xie, Q. Huang, C. Gao, Y. Wang, L. Wang, B. Yang, H. Su, L. Huang, W. Huang, *Adv. Mater.* **2018**, *30*, 1705256.
92. Y. Song, M. Lu, G. A. Mandl, Y. Xie, G. Sun, J. Chen, X. Liu, J. A. Capobianco, L. Sun, *Angew. Chem., Int. Ed.* **2021**, *60*, 23790.
93. L. Liang, D. B. L. Teh, N. D. Dinh, W. Chen, Q. Chen, Y. Wu, S. Chowdhury, A. Yamanaka, T. C. Sum, C. H. Chen, N. V. Thakor, A. H. All, X. Liu, *Nat. Commun.* **2019**, *10*, 1391.
94. Y. Han, C. Gao, T. Wei, K. Zhang, Z. Jiang, J. Zhou, M. Xu, L. Yin, F. Song, L. Huang, *Angew. Chem., Int. Ed.* **2022**, *61*, e202212089.
95. X. Fu, S. Fu, Q. Lu, J. Zhang, P. Wan, J. Liu, Y. Zhang, C. H. Chen, W. Li, H. Wang, Q. Mei, *Nat. Commun.* **2022**, *13*, 4741.
96. a) E. Chaudan, J. Kim, S. Tusseau-Nenez, P. Goldner, O. L. Malta, J. Peretti, T. Gacoin, *J. Am. Chem. Soc.* **2018**, *140*, 9512; b) S. Shi, L. D. Sun, Y. X. Xue, H. Dong, K. Wu, S. C. Guo, B. T. Wu, C. H. Yan, *Nano Lett.* **2018**, *18*, 2964.
97. J. Hao, Y. Zhang, X. Wei, *Angew. Chem., Int. Ed.* **2011**, *50*, 6876.
98. Y. Wu, J. Xu, X. Qin, J. Xu, X. Liu, *Nat. Commun.* **2021**, *12*, 2022.
99. Y. Liu, D. Wang, J. Shi, Q. Peng, Y. Li, *Angew. Chem., Int. Ed.* **2013**, *52*, 4366.
100. J. Zhang, L. Dai, A. M. Webster, W. T. K. Chan, L. E. Mackenzie, R. Pal, S. L. Cobb, G. L. Law, *Angew. Chem., Int. Ed.* **2021**, *60*, 1004.
101. Y. Wang, J. Zhou, J. Gao, K. Zhang, C. Gao, X. Xie, L. Huang, *Ann. Phys.* **2019**, *531*, 1900026.
102. H. Dong, L. D. Sun, C. H. Yan, *J. Am. Chem. Soc.* **2021**, *143*, 20546.
103. A. De, R. Ranjan, *Phys. Rev. B* **2018**, *98*, 094111.
104. V. K. Tikhomirov, L. F. Chibotaru, D. Saurel, P. Gredin, M. Mortier, V. V. Moshchalkov, *Nano Lett.* **2009**, *9*, 721.
105. Y. Wang, J. Gao, C. Gao, H. Ma, B. Yang, Y. Han, E. Zhou, Q. Cheng, S. Jing, L. Huang, *Nanoscale* **2019**, *11*, 16562.
106. A. Borodziuk, M. Baranowski, T. Wojciechowski, R. Minikayev, B. Sikora, D. K. Maude, P. Plochocka, L. Klopotoski, *Nanoscale* **2020**, *12*, 20300.
107. Y. Du, Y. Jiang, T. Sun, J. Zhao, B. Huang, D. Peng, F. Wang, *Adv. Mater.* **2019**, *31*, 1807062.
108. X. Yang, X. Jin, A. Zheng, P. Duan, *ACS Nano* **2023**, *17*, 2661.
109. M. D. Wisser, M. Chea, Y. Lin, D. M. Wu, W. L. Mao, A. Salleo, J. A. Dionne, *Nano Lett.* **2015**, *15*, 1891.
110. K. Zhang, C. Gao, Z. Jiang, Y. Wei, Y. Pan, C. Wei, H. Li, K. Wang, B. Zou, L. Huang, *Adv. Opt. Mater.* **2019**, *8*, 1901031.
111. D. Tu, C. N. Xu, S. Kamimura, Y. Horibe, H. Oshiro, L. Zhang, Y. Ishii, K. Hyodo, G. Marriott, N. Ueno, X. G. Zheng, *Adv. Mater.* **2020**, *32*, 1908083.
112. Y. Wang, X. Yang, C. Liu, Z. Liu, Q. Fang, F. Bai, S. Wang, X. Hou, B. Feng, B. Chen, B. Zou, *Angew. Chem., Int. Ed.* **2022**, *61*, e202210836.
113. a) Y. G. Galyametdinov, A. A. Knyazev, V. I. Dzhabarov, T. Cardinaels, K. Driesen, C. Görrler-Walrand, K. Binnemans, *Adv. Mater.* **2008**, *20*, 252; b) S. Ye, Y. Teng, A. Juan, J. Wei, L. Wang, J. Guo, *Adv. Opt. Mater.* **2017**, *5*, 1600956.
114. H. He, J. Liu, K. Li, Z. Yin, J. Wang, D. Luo, Y. J. Liu, *Nano Lett.* **2020**, *20*, 4204.
115. X. Yang, M. Zhou, Y. Wang, P. Duan, *Adv. Mater.* **2020**, *32*, 2000820.
116. Y. Chen, H. Deng, X. Sha, W. Chen, R. Wang, Y. H. Chen, D. Wu, J. Chu, Y. S. Kivshar, S. Xiao, C. W. Qiu, *Nature* **2023**, *613*, 474.
117. a) W. Dong, H. Liu, J. K. Behera, L. Lu, R. J. H. Ng, K. V. Sreekanth, X. Zhou, J. K. W. Yang, R. E. Simpson, *Adv. Funct. Mater.* **2018**, *29*, 1806181; b) J. Tian, H. Luo, Y. Yang, F. Ding, Y. Qu, D. Zhao, M. Qiu, S. I. Bozhevolnyi, *Nat. Commun.* **2019**, *10*, 396; c) C. Choi, S. E. Mun, J. Sung, K. Choi, S. Y. Lee, B. Lee, *Adv. Funct. Mater.* **2020**, *31*, 2007210; d) A. Leitiss, A. Heßler, S. Wahl, M. Wuttig, T. Taubner, A. Tittl, H. Altug, *Adv. Funct. Mater.* **2020**, *30*, 1910259; e)

- Y. Zhao, Y. Yang, C. Ji, Q. Liang, H. Fu, X. Liu, L. Zhou, J. Li, Y. Wang, *Adv. Funct. Mater.* **2023**, *33*, 2214492.
118. a) J. Li, S. Kamin, G. Zheng, F. Neubrech, S. Zhang, N. Liu, *Sci. Adv.* **2018**, *4*, eaar6768; b) J. Li, Y. Chen, Y. Hu, H. Duan, N. Liu, *ACS Nano* **2020**, *14*, 7892.
  119. a) L. Cai, K. Du, Y. Qu, H. Luo, M. Pan, M. Qiu, Q. Li, *Opt. Lett.* **2018**, *43*, 1295; b) M. Zhang, M. Pu, F. Zhang, Y. Guo, Q. He, X. Ma, Y. Huang, X. Li, H. Yu, X. Luo, *Adv. Sci.* **2018**, *5*, 1800835; c) Y. Kim, P. C. Wu, R. Sokhoyan, K. Mauser, R. Glaudell, G. Kafaie Shirmanesh, H. A. Atwater, *Nano Lett.* **2019**, *19*, 3961; d) P. Pitchappa, A. Kumar, S. Prakash, H. Jani, T. Venkatesan, R. Singh, *Adv. Mater.* **2019**, *31*, 1808157; e) J. Faneca, L. Trimby, I. Zeimpekis, M. Delaney, D. W. Hewak, F. Y. Gardes, C. D. Wright, A. Baldycheva, *Opt. Express* **2020**, *28*, 16394; f) S. Qin, N. Xu, H. Huang, K. Jie, H. Liu, J. Guo, H. Meng, F. Wang, X. Yang, Z. Wei, *Opt. Express* **2021**, *29*, 7925; g) F. Z. Shu, J. N. Wang, R. W. Peng, B. Xiong, R. H. Fan, Y. J. Gao, Y. Liu, D. X. Qi, M. Wang, *Laser Photonics Rev.* **2021**, *15*, 2100155; h) B. Chen, S. Yang, J. Chen, J. Wu, K. Chen, W. Li, Y. Tan, Z. Wang, H. Qiu, K. Fan, C. Zhang, H. Wang, Y. Feng, Y. He, B. Jin, X. Wu, J. Chen, P. Wu, *Light Sci. Appl.* **2023**, *12*, 136.
  120. F. Zhang, X. Xie, M. Pu, Y. Guo, X. Ma, X. Li, J. Luo, Q. He, H. Yu, X. Luo, *Adv. Mater.* **2020**, *32*, 1908194.
  121. a) H.-S. Ee, R. Agarwal, *Nano Lett.* **2016**, *16*, 2818; b) P. Gutruf, C. Zou, W. Withayachumnankul, M. Bhaskaran, S. Sriram, C. Fumeaux, *ACS Nano* **2016**, *10*, 133; c) S. M. Kamali, E. Arbabi, A. Arbabi, Y. Horie, A. Faraon, *Laser Photonics Rev.* **2016**, *10*, 1002; d) D. Wang, M. R. Bourgeois, W. K. Lee, R. Li, D. Trivedi, M. P. Knudson, W. Wang, G. C. Schatz, T. W. Odom, *Nano Lett.* **2018**, *18*, 4549; e) C. Zhang, J. Jing, Y. Wu, Y. Fan, W. Yang, S. Wang, Q. Song, S. Xiao, *ACS Nano* **2020**, *14*, 1418; f) X. Zhang, Y. Zhou, H. Zheng, A. E. Linares, F. C. Ugwu, D. Li, H. B. Sun, B. Bai, J. G. Valentine, *Nano Lett.* **2021**, *21*, 8715; g) J. Yu, Z. Liu, M. Wang, C. Wang, G. Chen, Z. Cui, T. Wang, H. Yang, X. Wang, X. Chen, *Adv. Mater.* **2022**, *34*, 2102560.
  122. A. Karvounis, N. Aspiotis, I. Zeimpekis, J. Y. Ou, C. C. Huang, D. Hewak, N. I. Zheludev, *Adv. Sci.* **2019**, *6*, 1900974.
  123. W. F. Chiang, H. M. Silalahi, Y. C. Chiang, M. C. Hsu, Y. S. Zhang, J. H. Liu, Y. Yu, C. R. Lee, C. Y. Huang, *Opt. Express* **2020**, *28*, 27676.
  124. X. Zhuang, W. Zhang, K. Wang, Y. Gu, Y. An, X. Zhang, J. Gu, D. Luo, J. Han, W. Zhang, *Light Sci. Appl.* **2023**, *12*, 14.
  125. a) S. Sun, W. Yang, C. Zhang, J. Jing, Y. Gao, X. Yu, Q. Song, S. Xiao, *ACS Nano* **2018**, *12*, 2151; b) W. Yang, S. Xiao, Q. Song, Y. Liu, Y. Wu, S. Wang, J. Yu, J. Han, D. P. Tsai, *Nat. Commun.* **2020**, *11*, 1864; c) Z. Li, C. Wan, C. Dai, J. Zhang, G. Zheng, Z. Li, *Adv. Opt. Mater.* **2021**, *9*, 2100297.
  126. a) J. Lu, B. Sain, P. Georgi, M. Protte, T. Bartley, T. Zentgraf, *Adv. Opt. Mater.* **2021**, *10*, 2101781; b) C. Jung, S. J. Kim, J. Jang, J. H. Ko, D. Kim, B. Ko, Y. M. Song, S. H. Hong, J. Rho, *Sci. Adv.* **2022**, *8*, eabm8598; c) S. Wan, C. Dai, Z. Li, L. Deng, Y. Shi, W. Hu, G. Zheng, S. Zhang, Z. Li, *Adv. Sci.* **2023**, *10*, 2205581.
  127. a) J. Karst, M. Floess, M. Ubl, C. Dingler, C. Malacrida, T. Steinle, S. Ludwigs, M. Hentschel, H. Giessen, *Science* **2021**, *374*, 612; b) W. Yang, G. Qu, F. Lai, Y. Liu, Z. Ji, Y. Xu, Q. Song, J. Han, S. Xiao, *Adv. Mater.* **2021**, *33*, 2101258; c) Q. Li, J. van de Groep, A. K. White, J. H. Song, S. A. Longwell, P. M. Fordyce, S. R. Quake, P. G. Kik, M. L. Brongersma, *Nat. Nanotechnol.* **2022**, *17*, 1097.
  128. a) Y. Lee, M.-K. Park, S. Kim, J. H. Shin, C. Moon, J. Y. Hwang, J.-C. Choi, H. Park, H.-R. Kim, J. E. Jang, *ACS Photonics* **2017**, *4*, 1954; b) S. Q. Li, X. Xu, R. Maruthiyodan Veetil, V. Valucas, R. Paniagua-Dominguez, A. I. Kuznetsov, *Science* **2019**, *364*, 1087; c) M. Bosch, M. R. Shcherbakov, K. Won, H. S. Lee, Y. Kim, G. Shvets, *Nano Lett.* **2021**, *21*, 3849; d) I. Kim, J. Jang, G. Kim, J. Lee, T. Badloe, J. Mun, J. Rho, *Nat. Commun.* **2021**, *12*, 3614; e) J. Wang, K. Li, H. He, W. Cai, J. Liu, Z. Yin, Q. Mu, V. K. S. Hisao, D. Gérard, D. Luo, G. Li, Y. J. Liu, *Laser Photonics Rev.* **2021**, *16*, 2100396; f) S. Mansha, P. Moitra, X. Xu, T. W. W. Mass, R. M. Veetil, X. Liang, S. Q. Li, R. Paniagua-Dominguez, A. I. Kuznetsov, *Light Sci. Appl.* **2022**, *11*, 141.
  129. a) L. Deng, J. Deng, Z. Guan, J. Tao, Y. Chen, Y. Yang, D. Zhang, J. Tang, Z. Li, Z. Li, S. Yu, G. Zheng, H. Xu, C. W. Qiu, S. Zhang, *Light Sci. Appl.* **2020**, *9*, 101; b) Q. Li, W. Bao, Z. Nie, Y. Xia, Y. Xue, Y. Wang, S. Yang, X. Zhang, *Nat. Photon.* **2021**, *15*, 267; c) P. Zheng, Q. Dai, Z. Li, Z. Ye, J. Xiong, H. C. Liu, G. Zheng, S. Zhang, *Sci. Adv.* **2021**, *7*, eabg0363; d) M. Song, L. Feng, P. Huo, M. Liu, C. Huang, F. Yan, Y. Q. Lu, T. Xu, *Nat. Nanotechnol.* **2023**, *18*, 71; e) P. Huo, M. Song, W. Zhu, C. Zhang, L. Chen, H. J. Lezec, Y. Lu, A. Agrawal, T. Xu, *Optica* **2020**, *7*, 1171.
  130. A. C. Overvig, S. Shrestha, S. C. Malek, M. Lu, A. Stein, C. Zheng, N. Yu, *Light Sci. Appl.* **2019**, *8*, 92.
  131. Z. Shen, S. Zhou, X. Li, S. Ge, P. Chen, W. Hu, Y. Lu, *Adv. Photonics* **2020**, *2*, 036002.
  132. Y. Hu, X. Ou, T. Zeng, J. Lai, J. Zhang, X. Li, X. Luo, L. Li, F. Fan, H. Duan, *Nano Lett.* **2021**, *21*, 4554.
  133. a) I. Kim, M. A. Ansari, M. Q. Mehmood, W. S. Kim, J. Jang, M. Zubair, Y. K. Kim, J. Rho, *Adv. Mater.* **2020**, *32*, 2004664; b) J. Li, P. Yu, S. Zhang, N. Liu, *Nat. Commun.* **2020**, *11*, 3574.
  134. a) H. Chung, O. D. Miller, *ACS Photonics* **2020**, *7*, 2236; b) A. Lininger, A. Y. Zhu, J. S. Park, G. Palermo, S. Chatterjee, J. Boyd, F. Capasso, G. Strangi, *Proc. Natl. Acad. Sci. U. S. A.* **2020**, *117*, 20390.

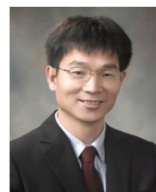
## AUTHOR BIOGRAPHIES



**Ling-Ling Ma** is currently an assistant professor in the College of Engineering and Applied Sciences at Nanjing University, China. She received her Ph.D. from Nanjing University in 2019. Her research focuses on self-assembled liquid crystal materials, particularly photo-patterned liquid crystalline hierarchical architectures, self-propelling liquid crystal actuators, and soft-matter photonics.



**Yu Wang** is currently an associate professor in the College of Engineering and Applied Sciences at Nanjing University. He received his B.S. degree from Tongji University (2010) and Ph.D. degree from Fudan University (2015). Before joining Nanjing University, he worked as a postdoctoral associate at Tufts University (2015–2020). His research focuses on developing biomass-based soft, smart, and sustainable optical materials and devices.



**Ling Huang** received his Ph.D. degree from Nanjing University in 2001. He pursued post-doctoral researches at the University of California, Berkeley (Gabor A. Somorjai) in 2001, Florida State University (Seunghun Hong) in 2002, and Northwestern University (Chad A. Mirkin) in 2004. Dr. Huang joined Nanyang Technological University, Singapore, as an associate professor in 2009 after 1 year of working at Corning Incorporated as a senior research scientist in 2008. He



relocated to Nanjing Tech University in 2012 and then joined Xinjiang University since 2021. His current research focuses on the optical, electronic, and catalytic properties of rare earth, especially scandium-based, nanomaterials.



**Yan-Qing Lu** is currently a Changjiang distinguished professor at Nanjing University and a fellow of the Optical Society of America, Chinese Optical Society, and Chinese Society for Optical Engineering. He received both his B.S. and Ph.D. degrees from Nanjing University, China, in 1991 and 1996, respectively.

He has 5 years of experience in telecom industries in the United States and China. His research interests include artificial microstructures and their optoelectronic applications, particularly in liquid crystal photonics, bionic metamaterials, fiber optics, and nonlinear optics.

**How to cite this article:** R. Zheng, Y. Wei, Z.-C. Zhang, Z.-Y. Wang, L.-L. Ma, Y. Wang, L. Huang, Y.-Q. Lu, *Responsive Mater.* **2023**, *1*, e20230017. <https://doi.org/10.1002/rpm.20230017>